Intercomparison and closure calculations using measurements of aerosol species and optical properties during the Yosemite Aerosol Characterization Study

William C. Malm,[1] Derek E. Day,[2] Christian Carrico,[3] Sonia M. Kreidenweis,[3] Jeffrey L. Collett Jr.,[3] Gavin McMeeking,[3] Taehyoung Lee,[3] Jacqueline Carrillo,[3] and Bret Schichtel[1]

Received 5 October 2004; revised 24 March 2005; accepted 11 April 2005; published 19 July 2005.

[1] Physical and optical properties of inorganic aerosols have been extensively studied, but less is known about carbonaceous aerosols, especially as they relate to the non-urban settings such as our nation's national parks and wilderness areas. Therefore an aerosol characterization study was conceived and implemented at one national park that is highly impacted by carbonaceous aerosols, Yosemite. The primary objective of the study was to characterize the physical, chemical, and optical properties of a carbon-dominated aerosol, including the ratio of total organic matter weight to organic carbon, organic mass scattering efficiencies, and the hygroscopic characteristics of a carbon-laden ambient aerosol, while a secondary objective was to evaluate a variety of semi-continuous monitoring systems. Inorganic ions were characterized using 24-hour samples that were collected using the URG and Interagency Monitoring of Protected Visual Environments (IMPROVE) monitoring systems, the micro-orifice uniform deposit impactor (MOUDI) cascade impactor, as well as the semi-continuous particle-into-liquid sampler (PILS) technology. Likewise, carbonaceous material was collected over 24-hour periods using IMPROVE technology along with the thermal optical reflectance (TOR) analysis, while semi-continuous total carbon concentrations were measured using the Rupprecht and Patashnick (R&P) instrument. Dry aerosol number size distributions were measured using a differential mobility analyzer (DMA) and optical particle counter, scattering coefficients at near-ambient conditions were measured with nephelometers fitted with PM_{10} and $PM_{2.5}$ inlets, and "dry" $PM_{2.5}$ scattering was measured after passing ambient air through Perma Pure Nafion® dryers. In general, the 24-hour "bulk" measurements of various aerosol species compared more favorably with each other than with the semi-continuous data. Semi-continuous sulfate measurements correlated well with the 24-hour measurements, but were biased low by about 0.15 $\mu g/m^3$. Semi-continuous carbon concentrations did not compare favorably with 24-hour measurements. Fine mass closure calculations suggested that the factor for estimating organic mass from measurements of carbon was approximately 1.8. Furthermore, fine scattering closure calculations showed that the use of 4.0 m^2/g for the fine organic mass scattering coefficient was an underestimate by at least 30% for periods with high organic mass concentrations.

Citation: Malm, W. C., D. E. Day, C. Carrico, S. M. Kreidenweis, J. L. Collett Jr., G. McMeeking, T. Lee, J. Carrillo, and B. Schichtel (2005), Intercomparison and closure calculations using measurements of aerosol species and optical properties during the Yosemite Aerosol Characterization Study, *J. Geophys. Res.*, *110*, D14302, doi:10.1029/2004JD005494.

1. Introduction

[2] Atmospheric aerosols, natural and anthropogenic, alter the radiative properties of the atmosphere through their scattering and absorptive characteristics. Understanding these properties is essential to estimating their role on visibility impairment and climate forcing [*Penner et al.*, 1992; *Iacobellis et al.*, 1999; *U.S. Environmental Protection Agency*, 1999; *Malm et al.*, 2004]. Over the years, physical and optical properties of inorganic aerosols have been extensively studied, but less is known about carbonaceous aerosols, especially as they relate to the non-urban setting

[1]National Park Service-Air Resources Division, Cooperative Institute for Research in the Atmosphere, Colorado State University, Fort Collins, Colorado, USA.
[2]Cooperative Institute for Research in the Atmosphere, Colorado State University, Fort Collins, Colorado, USA.
[3]Department of Atmospheric Science, Colorado State University, Fort Collins, Colorado, USA.

0148-0227/05/2004JD005494$09.00

such as our nation's national parks and wilderness areas [*Seinfeld and Pandis*, 1998].

[3] A number of studies assessing aerosol physical and optical properties have been, and in some cases continue to be, carried out in the non-urban setting [*Zhang et al.*, 1993; *Dick et al.*, 2000; *Malm and Day*, 2000; *Malm et al.*, 2000; *Hand et al.*, 2002]. However, in most cases ambient mass concentrations are dominated by aerosols other than carbonaceous material. Because carbonaceous material was not the dominant aerosol species, it was difficult to "tease out" its physio-chemical-optical properties such as growth factors or enhanced scattering as a function of relative humidity. Therefore an aerosol characterization study was conceived and implemented at one national park that is highly impacted by carbonaceous aerosols, Yosemite.

[4] On the average, carbonaceous material contributes about 50–60% of the fine (<2.5 μm) aerosols, and during the fall season that percentage can be in excess of 80%. The overall objective of the study was to characterize the physical, chemical, and optical properties of a carbon-dominated aerosol including the ratio of total organic matter weight to organic carbon, organic mass scattering efficiencies, and the hygroscopic characteristics of a carbon-laden ambient aerosol. Secondary objectives were to evaluate a variety of semi-continuous monitoring systems and identify the sources of carbonaceous material (biogenic vs. anthropogenic, primary vs. secondary) with an eye toward understanding how wild and prescribed fire related activities contribute to carbon mass concentrations [*Brown et al.*, 2002; *Bench and Herckes*, 2004]. The study was conducted from 15 July to 4 September 2002 at Turtleback Dome on the south rim of the entrance to Yosemite Valley at the Interagency Monitoring of Protected Visual Environments (IMPROVE) monitoring site at 119.70 W; Lat 37.71 N; Elevation 1615m. The overall study is described fully by *Carrico et al.* [2005].

[5] It is customary to estimate organic mass concentrations from measurements of organic carbon mass by multiplying a factor which is the assumed ratio between average molecular weight and carbon weight. This factor has been discussed in some detail by *Turpin and Lim* [2001] and will not be repeated here. Based on measurements that extend back to 1977 [*White and Roberts*, 1977] a factor of between 1.2 and 1.4 has quite often been used. The regional guidance document for tracking progress of visibility change over time [*U.S. Environmental Protection Agency*, 2003] has adopted a 1.4 factor. Turpin, based to a large degree on laboratory and field measurement of various organic aerosol species, has concluded that a factor of about 1.6 would be appropriate for an urban organic aerosol while a factor of 2.1 may be more appropriate for an aged, non-urban aerosol.

[6] White in *Trijonis et al.* [1990] estimated, based on 30 field studies, a range of feasible dry mass scattering efficiencies for sulfates and organic aerosols. A low of 1.9 to a high of 6.1 m^2/g was estimated for sulfates while a range of 1.3 to 7.0 m^2/g was estimated for organics. Nominal values of mass scattering efficiencies of 3.0 m^2/g and 4.0 m^2/g for sulfates and organics, respectively, have been adopted by the Environmental Protection Agency (EPA) [*U.S. Environmental Protection Agency*, 1999] for tracking visibility changes over time that are based on aerosol measurements. *Malm and Pitchford* [1997], *Malm et al.* [2000], and *Malm et al.* [2003] have reported average summertime sulfate mass scattering efficiencies, based on mass size distribution measurements, of 2.03, 2.23, 3.1, 2.63, and 2.4 m^2/g for Lake Mead National Recreation Area, and Grand Canyon, Big Bend, Shenandoah, and Great Smoky national parks, respectively. At Lake Mead and Grand Canyon no relationship was found between sulfate mass concentrations and mass scattering efficiencies, while at Big Bend and the eastern national parks a weak positive relationship between mass concentration and scattering efficiency was observed that ranged from about 2.0–5.0 m^2/g. Little data on mass scattering efficiencies for organic carbon aerosols have been reported primarily because of the inability to accurately measure mass size distributions of organic carbon aerosols and the lack of information on organic aerosol refractive index.

[7] This paper will focus on the intercomparability of various sampling systems, the uncertainty associated with semi-continuous measurements of carbon and inorganic species, and through the use of mass and scattering closure calculations, on the factor for estimating the average molecular weight of particulate organic matter from carbon weight and organic carbon mass scattering efficiencies.

2. Experimental Methods

[8] A wide variety of instrumentation was used during the Yosemite study. Aerosol physical, chemical, and optical properties were characterized using the following samplers and instruments.

2.1. Characterization of Aerosol Chemical Composition

[9] The chemical composition of ambient aerosols during the Yosemite study was characterized using several different aerosol samplers and analytical techniques. These samplers were operated on sample collection periods ranging from five minutes to more than 24 hours. Fine (<2.5 μm) and coarse (<10 μm) organic carbon, inorganic compounds, elemental carbon, and the concentration of most elements were measured during this field study. A brief description of each sampling system used during the Yosemite study is given below and summarized in Table 1.

2.1.1. IMPROVE Sampler

[10] Two sets of IMPROVE [*Malm et al.*, 1994] samplers were used during this study. In the IMPROVE monitoring system described by *Malm et al.* [1994], the x-ray fluorescence (XRF) analysis was carried out under a well-defined protocol (http://vista.cira.colostate.edu/improve/Publications/SOPs/ucdavis_sops/sop301.pdf); however, for this study the XRF analysis was done at the Lawrence Livermore National Laboratory [*Bench et al.*, 2001]. The two IMPROVE sampler systems at Turtleback Dome consisted of three modules or channels. Each channel has its own filter and sample inlet; however, a single computer controls all channels. Typically the channels are referred to as A (from which aerosol gravimetric mass and elements Na-Pb are measured), B (from which ions are measured), and C (analyzed for carbon by thermal optical reflectance (TOR)) [*Chow et al.*, 1993]. Samples were collected for 24 hours beginning at 0800 PST.

Table 1. Summary of Chemical Analyses

Sampler/Instrument and Size cut	Species Measured	Substrate	Denuder	Time	Analytical Technique
IMPROVE $PM_{2.5}$ Chan A	Elements, Mass	Teflon	None	24-hour	XRF, Gravimetric
IMPROVE $PM_{2.5}$ Chan B	Anions	Nylon	Na_2CO_3	24-hour	Ion Chromatography
IMPROVE $PM_{2.5}$ Chan C	Carbon	Quartz	None	24-hour	TOR
IMPROVE PM_{10} Chan A	Elements, Mass	Teflon	None	24-hour	XRF, Gravimetric
IMPROVE PM_{10} Chan B	Anions	Nylon	Na_2CO_3	24-hour	Ion Chromatography
IMPROVE PM_{10} Chan C	Carbon	Quartz	None	24-hour	TOR
URG $PM_{2.5}$	Ions	Teflon Primary Nylon Backup	Na_2CO_3/H_3PO_3	24-hour and 6-hour during Intensives	Ion Chromatography
MOUDI multi-stage impactor	Ions	Aluminum Foil Teflon After-filter	None	24-hour and 12-hour Intensives	Ion Chromatography
PILS $PM_{2.5}$	Ions	None	$NaCO_3/H_3PO_4$	15-min	Ion Chromatography
R&P $PM_{2.5}$	Total Carbon	Stainless Steel Impactor	None	1-hour	Thermal Desorption
Aethalometer $PM_{2.5}$	Black Carbon	Quartz	None	5-min	Light Absorption

2.1.2. URG Sampler

[11] The URG sampling system [*Lee et al.*, 2004] employed during the Yosemite study consisted of a 2.5 μm cyclone, two denuders coated with Na_2CO_3 and H_3PO_3 to remove nitric acid and ammonia gas, respectively, a Teflo® primary filter for particle collection, and a nylon backup filter to collect any nitrate which escaped from the primary filter. Samples were collected for 24 hours beginning at 0800 PST; however, during a few periods (intensives) 6-hour samples were collected. Filter extracts were analyzed by ion chromatography for major ions including SO_4^{2-}, NO_3^-, Cl^-, Na^+, K^+, Ca^{2+}, Mg^{2+}, NH_4^+, and oxalate.

2.1.3. MOUDI

[12] The micro-orifice uniform deposit impactor (MOUDI) [*Marple et al.*, 1991] sampler is a cascade impactor, which selectively collects particles in discrete size ranges. The MOUDI system is used to collect aerosol mass in nine size ranges and includes an after-filter which collects all those aerosols less than 0.018 μm. During the Yosemite study, aerosol samples were collected for 24-hour durations except during intensives when 12-hour samples were collected. Coated aluminum foil was used as a substrate while the after-filter was Teflo®. Analyses of sample extracts were done by ion chromatography for major anions (SO_4^{2-}, NO_3^-, Cl^-) and major cations (NH_4^+, Na^+, Ca^{2+}, K^+).

2.1.4. PILS

[13] The particle-into-liquid sampler (PILS) [*Orsini et al.*, 2003] was operated continuously during the Yosemite study to obtain the concentration of major ions (Na^+, K^+, Ca^{2+}, Mg^{2+}, Cl^-, NO_3^-, and SO_4^{2-}) with a time resolution of 15 minutes. This system introduces atmospheric particles into a supersaturated environment by mixing the airflow with 100°C steam, which grows the particles large enough to be collected by an impactor. The droplets are washed off the impactor and collected in a flowing liquid stream, which is analyzed by ion chromatography. An internal LiBr standard is used to account for dilution by condensed steam.

2.1.5. R&P Carbon Analyzer

[14] A Rupprecht and Patashnick model 5400 ambient carbon particulate monitor [*Rupprecht et al.*, 1995] was used to measure aerosol total carbon (TC). This instrument collects sample aerosol on one of two stainless steel impactor plates. After sample collection, the impactor plate is heated to 750°C in air and the CO_2 evolved is measured with a Li-Cor sensor. Sampling and heating are alternated between the two impactors. A 2.5 μm size cut inlet was installed in front of the sample line, while the minimum size cut for the impactors is 0.14 μm with a flow of 16.7 lpm. Hourly samples were analyzed for TC only, as it was determined that one hour did not provide enough time for a two temperature step elemental carbon (EC) and organic carbon (OC) analysis when concentrations of carbon were at their lowest levels. Furthermore, it was assumed that by heating the impaction surface to 50°C, gases would not adsorb to its surface and therefore the instrument was operated without a gas denuder.

2.1.6. Aethalometer

[15] A two-channel aethalometer [*Hansen et al.*, 1984] was used to measure aerosol absorption at two wavelengths. The 880 nm wavelength is used to infer aerosol black carbon (BC) concentration, while a second ultraviolet (370 nm) channel is sensitive to absorption both by black carbon and by certain organic compounds present in wood smoke and diesel exhaust. A difference in signal strength between the two channels implies the presence of wood smoke or diesel. An aerosol sample is collected on quartz fiber filter tape and the attenuation of the light beam at the specified wavelengths is measured. The instrument was run with a 2.5 μm cyclone in front of the sample line and a 5-minute measurement frequency. For purposes of this analysis, black carbon derived from the aethalometer will be interpreted in the same way as elemental carbon derived from the TOR analysis.

2.2. Optical Instrumentation

[16] Several optical instruments were operated during the Yosemite study to measure aerosol light scattering, light extinction, dry aerosol light scattering, and light scattering as a function of relative humidity. The ambient light scattering coefficient was measured using two standard Optec nephelometers [*Molenar*, 1997] and two Optec nephelometers fitted with 2.5 μm cutpoint cyclones, all having an effective wavelength sensitivity of 550 nm. The ambient light extinction coefficient at 550 nm was measured continuously using an Optec LPV-2 transmissometer [*Molenar et al.*, 1989]. The aerosol light scattering coefficient was measured using two Radiance Research M903 nephelometers that measure scattering at an effective wavelength of 530 nm [*Day and Malm*, 2001]. One of these nephelometers was operated dry (reference signal), while the second

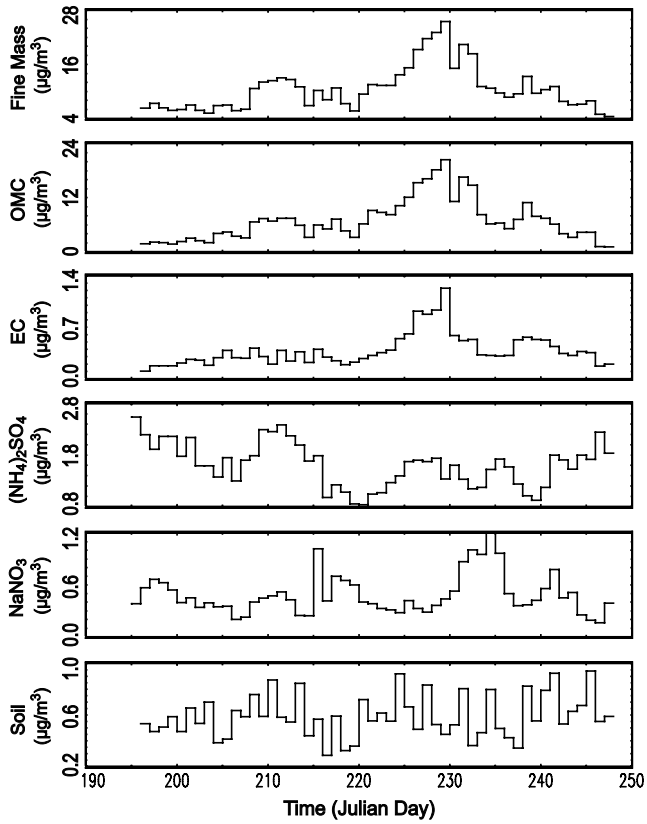

Figure 1. Temporal plot of fine gravimetric and the five major fine aerosol species mass concentrations.

nephelometer measured aerosol light scattering over a range of humidity (generally 10–90% RH). Aerosol humidity was controlled using Perma Pure Nafion® dryers.

2.3. Aerosol Particle Size

[17] Ambient aerosol was sampled through a flow splitter to deliver a common aerosol sample to the particle sizing instrumentation. Dry size distributions were measured with an electrical mobility technique (40 nm < D < 850 nm using TSI, Inc., models 3081 and 3010), a time of flight technique (aerodynamic 0.6 < D < 20 μm using TSI, Inc., Model 3320) and an optical sizing technique (0.1 < D < 2 μm using Particle Measuring Systems, Inc., LASAIR 1002 and 1003) [*Hering and McMurry*, 1991; *Sachweh et al.*, 1998; *Armendariz and Leith*, 2002; *Hand et al.*, 2002; *McMeeking et al.*, 2005]. Aerosol drying was accomplished using Nafion® membrane driers (Perma Pure Inc.) for the optical and electrical mobility analyzers and heating (T ~ 35C) for time of flight measurement. One of the optical particle counters measured unconditioned aerosol from the flow splitter. Examination of the overlapping regions for these measurements yields information on the refractive index and density [*Stolzenburg et al.*, 1998; *Hand and Kreidenweis*, 2002; *Hand et al.*, 2002].

3. Major Aerosol Species

[18] Figure 1 presents timelines of gravimetric fine mass, sulfate as ammonium sulfate, nitrate as sodium nitrate, organic mass carbon (OMC), elemental carbon (EC), and soil mass. Fine mass, organic mass, elemental carbon, and soil were derived from the IMPROVE sampling system while sulfates and nitrates are associated with the URG monitors. There are two elevated concentration episodes, one centered around Julian day 211, the other around Julian day 230, both of which are dominated by carbonaceous mass.

3.1. Comparison of Species Mass Concentrations as Measured by Various Sampling Configurations

[19] The tables referred to in this section contain statistical summaries of various species concentrations as derived by different sampling methodologies. The summaries include the mean, standard deviation, maximum, and minimum concentrations, the uncertainty (UNC) associated with the average value, and, under "Valid", the number of data points used in the analysis. The number of valid data points corresponds to the number of sampling periods for which all variables were analyzed. For example, only 25 MOUDI samples out of a possible 53 were submitted for chemical analysis, so statistical summaries are only presented for the sampling days that are in common with MOUDI samples. The average uncertainty was derived from the reported individual sampling period uncertainties (http://vista.cira.colostate.edu/improve/Publications/SOPs/ucdsop.asp). The uncertainties for the 24-hour average filter-based measurements of $PM_{2.5}$ and PM_{10} are better established than for the semi-continuous measurements such as the PILS inorganic and R&P carbon measurements or the MOUDI-derived ion mass concentrations. Therefore the mean of the bulk 24-hour samples will be used as a "standard" against which semi-continuous measurements will be compared. Some effort will be made to estimate the accuracy and precession of the semi-continuous techniques. This approach is somewhat different from the approach taken by *Weber et al.* [2003] and *Lim et al.* [2003] where they compared various individual semi-continuous measurements of aerosol species to the mean of species concentrations derived from all measurements. Their approach addresses intersampler variability and to some degree precision but does not address accuracy. Both additive and multiplicative biases will be explored through simple correlation tables between concentrations measured using the various sampling systems and ordinary least squares (OLS) regression analysis.

3.1.1. Sulfate and Sulfur

[20] Table 2b presents summary statistics for sulfate or sulfur as measured using either the IMPROVE, URG, MOUDI, or PILS sampling systems while Table 2a shows a correlation table of the same variables. The minimum detection limit (MDL) for these systems is on the order of 0.01–0.02 μg/m^3.

Table 2a. Correlation Table of Sulfate or Sulfur Mass Concentrations Derived From Various Sampling and Analytic Methodologies

Sulfate (0.0–2.5 μm)	XRF Sulfur*3	URG SO_4^{2-}	MOUDI SO_4^{2-}	PILS SO_4^{2-}
IMPROVE SO_4^{2-}	0.96	0.98	0.96	0.70
XRF Sulfur*3	NA	0.97	0.98	0.68
URG SO_4^{2-}	NA	NA	0.96	0.74
MOUDI SO_4^{2-}	NA	NA	NA	0.67

Table 2b. Statistical Summary of Sulfate or Sulfur Mass Concentration Derived From Various Sampling and Analytic Methodologies

Variable, $\mu g/m^3$	Mean	UNC	Std Dev	Minimum	Maximum	Valid
IMPROVE SO_4^{2-} (0.0–2.5)	1.11	0.011	0.31	0.56	1.55	25
XRF Sulfur*3 (0.0–2.5)	0.92	0.003	0.27	0.45	1.37	25
URG SO_4^{2-} (0.0–2.5)	1.20	0.005	0.33	0.61	1.73	25
MOUDI SO_4^{2-} (0.18–2.5)	1.09	0.014	0.32	0.57	1.64	25
After-filter SO_4^{2-} (<0.18)	0.30	0.005	0.27	0.05	0.83	25
PILS SO_4^{2-} (0.0–2.5)	1.09	0.03	0.35	0.48	2.01	25
IMPROVE Coarse SO_4^{2-}	0.00	0.011	0.04	−0.07	0.09	25
MOUDI Coarse SO_4^{2-}	0.79	0.018	0.17	0.49	1.08	25

[21] The discrete mass size distributions derived using the MOUDI system were smoothed using the Twomey inversion method. The ion mass concentration for MOUDI mass size distribution data was summed to 2.5 μm, allowing for an estimate of aerosol mass that corresponds to the 2.5 μm inlets on the other sampling configurations.

[22] The average of the IMPROVE and URG sulfate mass concentrations is 1.16 $\mu g/m^3$. It is this average that will be used as a reference value. The difference in sulfate mass as determined by these two systems is about 8%, while the intervariable correlation is high at 0.98. It is of interest to point out that 8% is well outside the estimated uncertainty of the average values which are based on precision/accuracy values reported for the two monitoring systems (http://vista.cira.colostate.edu/improve/Publications/SOPs/arssop.asp) [*Lee et al.*, 2004]. The bias between the two samplers is multiplicative as opposed to an additive offset. IMPROVE elemental sulfur times three (3*S) is 17% lower than the reference value but still highly correlated with the URG sulfate at 0.97. MOUDI sulfate (including the after-filter) is 6% lower than the reference value but nearly the same as URG-derived sulfate. Notice that about 28% of the sulfate mass on the average is found on the after-filter, implying an ultra-fine sulfate mode that is less than the 0.18 μm cutpoint of the last MOUDI stage. This mode was more commonly observed in the July time frame.

[23] It is of interest to point out the large diurnal variability in sulfate concentration data as represented by PILS. PILS-derived sulfate compares favorably on the average in that it is only 6% lower than the reference value; however, Table 2a shows that correlations are high for all systems (>0.95) except for the PILS-derived sulfate concentrations. The correlation between PILS sulfate averaged to 24 hours and sulfate derived from other samplers is lowest at about 0.7. Furthermore, Figure 2a shows a temporal plot of the average of the URG and IMPROVE sulfate and PILS sulfate concentrations, while the light gray data points in Figure 2b present the corresponding scatter plot. The estimated range of uncertainty for the URG/IMPROVE sulfate concentrations are shown; however, they have not been established for the PILS-derived variables and therefore are not shown for this uncorrected dataset. Except for

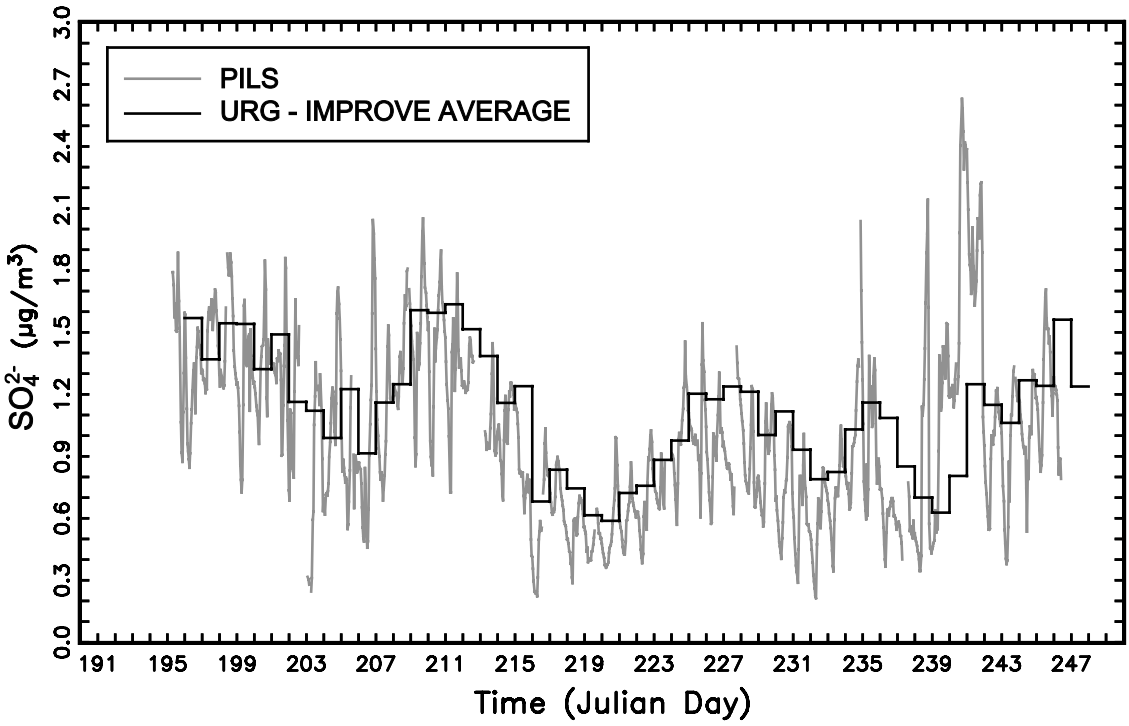

Figure 2a. Temporal plot of semi-continuous PILS and average URG/IMPROVE fine sulfate mass concentration.

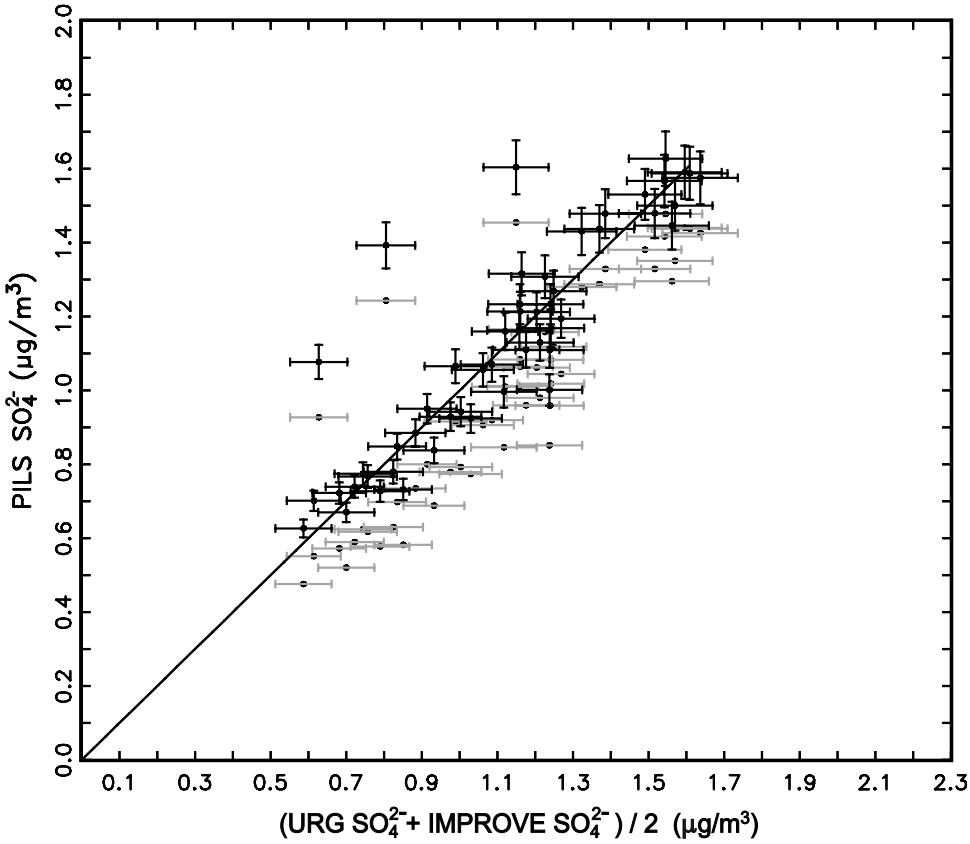

Figure 2b. Scatter plot of the average URG/IMPROVE and PILS fine sulfate mass concentrations. PILS data have been averaged to 24 hours for comparison to URG/IMPROVE samples. Data points in gray are for the measured data sets while those in black correspond to the bias-corrected PILS data.

three outlying data points, there is an additive offset between the two systems with sulfate derived from the PILS system being about 0.15 μg/m^3 lower across all sampling periods. The root mean square (RMS) error between the URG/IMPROVE and PILS sulfate is 0.18, while the RMS error of the URG/IMPROVE system is 0.085. Therefore an estimate of the overall RMS error of the PILS system is about 0.16. However, if the PILS data is corrected for the 0.15 μg/m^3 bias, the PILS RMS error is only 0.05, indicating that the precision of the PILS system is quite good. Figure 2b also shows a scatter plot of the URG/IMPROVE and bias-corrected PILS data sets along with the corrected or bias-removed estimated PILS uncertainty.

3.1.2. Nitrate

[24] Tables 3a and 3b present correlation coefficients and summary statistics for nitrate measured by the various sampling systems. The IMPROVE and URG nitrate values compare more favorably with each other than with other sampling systems. The difference between these two sampling methodologies for $PM_{2.5}$ nitrate is about 18% with an average of 0.36 μg/m^3. These variables correlate well at 0.98 and an OLS regression shows about a 0.04 μg/m^3 additive offset and a multiplicative bias of about 6%.

[25] $PM_{2.5}$ MOUDI nitrate is about 50% lower than this average. On the other hand, the difference between nitrate in the coarse mode as measured by MOUDI and IMPROVE is only 14%. Most nitrate in the coarse mode is in the form of sodium nitrate, while in the fine mode it is ammonium nitrate (see section 4 on Mass Size Distribution of Ionic Species). Possibly the larger difference between fine mode MOUDI and URG/IMPROVE reflects volatilization of nitrate from the aluminum impaction surfaces used in the MOUDI.

[26] Finally, PILS nitrate is about 22% lower than the URG/IMPROVE average; however, its correlation with either URG or IMPROVE nitrate is high at 0.83–0.84. A scatter plot of URG/IMPROVE average and PILS nitrate (Figure 3) shows PILS nitrate values are biased additively and multiplicatively low at about 0.02 μg/m^3 and 1.3 respectively. The root mean square error between the URG/IMPROVE and PILS nitrate is 0.11 while the RMS error of the URG/IMPROVE system is 0.045. Therefore an estimate of the overall RMS error of the PILS system is about 0.10 or 30%. However, if the PILS data is corrected for the additive and multiplicative bias, the RMS error between the URG/IMPROVE average and PILS nitrate is low at 0.05, implying that the PILS RMS error would be about 0.02. Therefore the implied precision of the PILS system is quite high. For reference the bias-corrected PILS

Table 3a. Correlation Table of Nitrate Mass Concentrations Derived From Various Sampling and Analytic Methodologies

Nitrate (0.0–2.5 μm)	URG NO_3^-	MOUDI NO_3^-	PILS NO_3^-
IMPROVE NO_3^-	0.98	0.78	0.84
URG NO_3^-	NA	0.81	0.83
MOUDI NO_3^-	NA	NA	0.63

Table 3b. Statistical Summary of Nitrate Mass Concentration Derived From Various Sampling and Analytic Methodologies

Variable, $\mu g/m^3$	Mean	UNC	Std Dev	Minimum	Maximum	Valid
IMPROVE NO_3^- (0.0–2.5)	0.32	0.004	0.17	0.14	0.75	25
URG NO_3^- (0.0–2.5)	0.39	0.006	0.17	0.16	0.88	25
MOUDI NO_3^- (0.18–2.5)	0.18	0.006	0.09	0.07	0.43	25
After-filter NO_3^- (<0.18)	0.01	0.003	0.01	0.00	0.02	25
PILS NO_3^- (0.0–2.5)	0.28	0.014	0.16	0.03	0.09	25
IMPROVE Coarse NO_3^-	0.21	0.008	0.12	−0.08	0.46	25
MOUDI Coarse NO_3^-	0.18	0.006	0.09	0.06	0.43	25

vs. URG/IMPROVE nitrate values are also presented in Figure 3.

3.1.3. Chloride

[27] Tables 4a and 4b show correlations between sampling systems and summary statistics for the chloride ion. Chloride ion concentrations are sufficiently low as to be at or below the MDL (≈0.01 $\mu g/m^3$) for either the fine or coarse mode, although the uncertainty associated with the average values would imply that the averages associated with the different monitoring systems are statistically different from each other. The correlations of chloride ion concentrations between monitoring systems are low and even negative for some comparisons. The highest correlation is between MOUDI- and IMPROVE-derived chloride concentrations.

3.1.4. Ammonium

[28] Table 5 presents summary statistics for the ammonium ion. Note that cation analysis was only carried out for aerosol samples collected using the URG and MOUDI systems. The URG- and MOUDI-derived ammonium concentrations compare quite favorably in that the average difference is about 8% and the intersampler correlation is 0.93. As with sulfate, a substantial amount of ammonium, about 32%, is found on the MOUDI after-filter, implying a substantial ultra fine mode. It is interesting to note that, relative to the fine mode, a substantial amount of ammonium is also found in the coarse fraction.

3.1.5. Sodium

[29] Correlations and statistical summaries related to sodium are found in Tables 6a and 6b. The URG, MOUDI, and PILS sodium are water-soluble sodium ions while the IMPROVE sodium was derived from an XRF analysis. URG, MOUDI, and PILS sodium are nearly the same at 0.12, 0.13, and 0.11 $\mu g/m^3$, respectively. On the other hand, XRF sodium is 58% lower at 0.05 $\mu g/m^3$ but has the highest correlation coefficient (0.91) when compared to URG

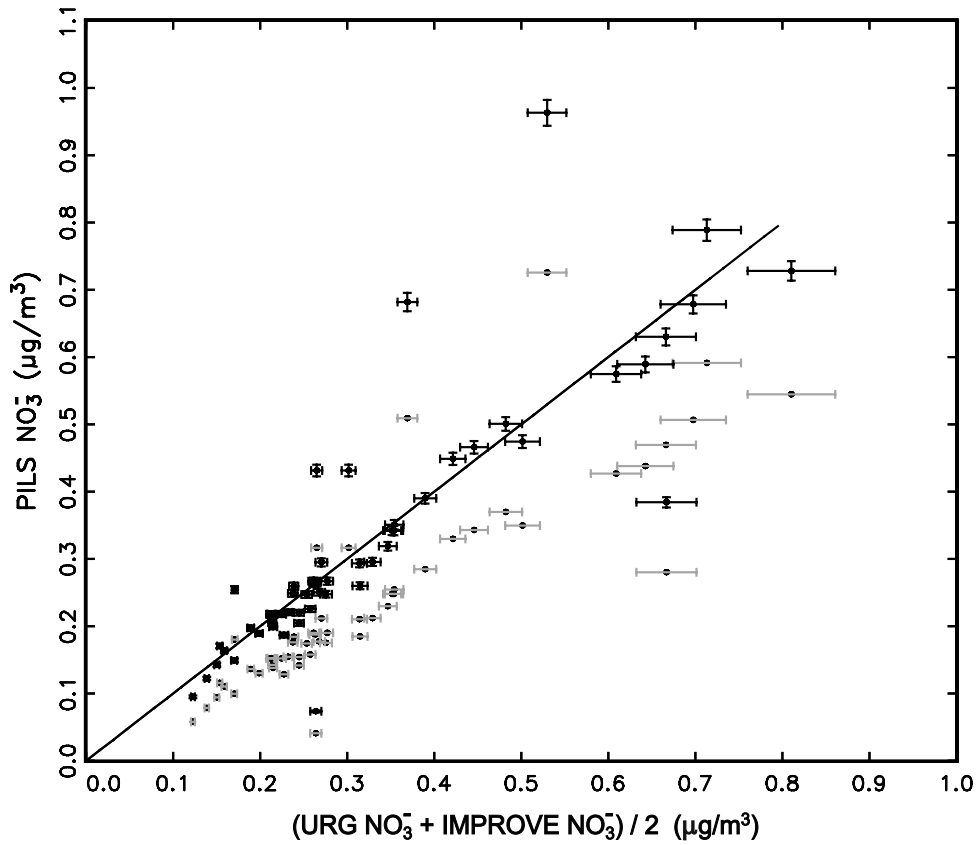

Figure 3. Scatter plot of the average URG/IMPROVE and PILS fine nitrate mass concentrations. PILS data have been averaged to 24 hours for comparison to URG/IMPROVE samples. Data points in gray are for the measured data sets while those in black correspond to the bias-corrected PILS data.

Table 4a. Correlation Table of Chloride Mass Concentrations Derived From Various Sampling and Analytic Methodologies

Chloride (0.0–2.5 μm)	URG Cl^-	MOUDI Cl^-	PILS Cl^-
IMPROVE Cl^-	0.15	0.44	−0.03
URG Cl^-	NA	−0.14	−0.11
MOUDI Cl^-	NA	NA	0.09

sodium, reflecting a substantial multiplicative bias. The correlation of PILS sodium with other sampling systems is between 0.6 and 0.7 with PILS sodium being additively biased low at about 0.15 $\mu g/m^3$.

3.1.6. Calcium

[30] As with the chloride, calcium concentrations are low at about 0.02–0.03 $\mu g/m^3$, uncorrelated, and near the MDL of about 0.02 $\mu g/m^3$ (see Tables 7a and 7b). As with sodium, the IMPROVE calcium concentrations are derived from an XRF analysis. The low correlation coefficients between calcium concentrations derived from different sampling systems are very low, reflecting concentrations that are at or near the MDL. Even though the average concentrations are similar, the low correlation between variables does not allow for a determination of whether the measurements are biased in an additive or multiplicative way.

3.1.7. Potassium

[31] As can be seen from Tables 8a and 8b, potassium derived from the various sampling systems compares quite favorably and is, on the average, about six times above the MDL of about 0.01 $\mu g/m^3$. The IMPROVE potassium concentrations are arrived at using an XRF analysis which includes water-soluble and soil potassium, while potassium derived from the other sampling systems is only the water-soluble component. The IMPROVE, URG, and MOUDI average potassium concentrations are, to two significant figures, the same. The fact that XRF-derived potassium (total potassium) agrees well with water-soluble potassium implies that most of the measured potassium is of the water-soluble kind. The average difference of 0.01 $\mu g/m^3$ between PILS K^+ and potassium derived by other methods is reflected as an additive bias. The correlation between IMPROVE, URG, and PILS potassium is 0.9 or greater, while MOUDI-derived potassium correlates with other sampling systems in the 0.5–0.6 range.

3.1.8. Carbon

[32] The R&P carbon analyzer was used to measure total carbon (TC) while an aethalometer was used to measure black carbon (BC) or elemental carbon (EC). BC from the aethalometer will be interpreted as being equivalent to EC derived from the TOR analysis. EC was a small, nearly constant fraction of the total carbon, which allowed for estimating the R&P OC by differencing the R&P total carbon and BC from the aethalometer. IMPROVE TOR EC and aethalometer BC differ by about 25% with IMPROVE TOR elemental carbon being the highest. For the IMPROVE system EC/TC = 0.10 while for the R&P/aethalometer system BC/TC = 0.05.

[33] Tables 9a and 9b contain correlations and summary statistics between $PM_{2.5}$ IMPROVE TOR and R&P TC, and IMPROVE TOR EC and aethalometer BC, while Figures 4a and 4b are temporal and scatter plots of R&P and IMPROVE TOR TC. First of all, note the elevated carbon concentrations as compared to inorganic ions. The TC carbon maximum concentration is about 12.5 $\mu g/m^3$ while sulfate peak concentrations were around 1.5 $\mu g/m^3$.

[34] Referring to the scatter plot it is clear that there is not an overall additive or multiplicative bias between the TOR- and R&P-derived TC values but rather the bias seems to be a function of concentration or possibly carbon mass composition. During the beginning and end of the study period, R&P TC is biased substantially higher (factors of 5 and 6) than IMPROVE TOR TC, while during the elevated carbon episode (JD = 225–230) it is biased slightly low. The correlation between the TC, EC, and BC variables is relatively high at 0.80–0.94. Although not shown here, the relationship between R&P and IMPROVE TOR organic mass is nearly the same as that of total carbon. Part of the observed discrepancy between IMPROVE TOR- and R&P-derived carbon may have been due to gases adsorbing on the impaction surface since the R&P instrument was operated without a denuder. Finally, about four times as much TC is found in the fine versus coarse mode while for elemental carbon the ratio is near 10. This substantial difference between these monitoring systems will be further explored with fine mass and scattering closure calculations.

4. Mass Size Distribution of Ionic Species

[35] Figure 5 shows a 24-hour average mass equivalent size distribution for selected ions on 31 August. There is a very interesting structure in the size distribution that is evident in almost every sample. Ammonium and sulfate ions tend to track each other and are usually found in the 0.1–2.0 μm size range, although in many cases there is as much or more mass on the after-filter (<0.18 μm) than the sum of sulfate/ammonium mass found on all MOUDI stages, implying an ultra fine mode of ammonium sulfate. On the average (see Table 10), 27% and 31% of the sulfate and ammonium mass, respectively, are found on the after-

Table 4b. Statistical Summary of Chloride Mass Concentration Derived From Various Sampling and Analytic Methodologies

Variable, $\mu g/m^3$	Mean	UNC	Std Dev	Minimum	Maximum	Valid
IMPROVE Cl^- (0.0–2.5)	−0.03	0.012	0.03	−0.08	0.01	24
URG Cl^- (0.0–2.5)	0.01	0.002	0.01	0.00	0.03	24
MOUDI Cl^- (0.18–2.5)	0.04	0.004	0.04	0.00	0.17	24
After-filter Cl^- (<0.18)	0.00	0.002	0.00	0.00	0.01	24
PILS Cl^- (0.0–2.5)	0.03	NA	0.02	0.01	0.07	24
IMPROVE Coarse Cl^-	0.01	0.005	0.04	−0.06	0.09	24
MOUDI Coarse Cl^-	0.04	0.004	0.04	0.00	0.17	24

Table 5. Statistical Summary of Ammonium Mass Concentration Derived From Various Sampling and Analytic Methodologies

Variable, $\mu g/m^3$	Mean	UNC	Std Dev	Minimum	Maximum	Valid
URG NH_4^+ (0.0–2.5)	0.48	0.002	0.11	0.26	0.65	25
MOUDI NH_4^+ (0.18–2.5)	0.52	0.010	0.13	0.28	0.78	25
After-filter NH_4^+ (<0.18)	0.17	0.004	0.13	0.04	0.42	25
MOUDI Coarse NH_4^+	0.36	0.010	0.09	0.20	0.53	25

Table 6b. Statistical Summary of Sodium Mass Concentration Derived From Various Sampling and Analytic Methodologies

Variable, $\mu g/m^3$	Mean	UNC	Std Dev	Minimum	Maximum	Valid
IMPROVE Na (0.0–2.5)	0.05	0.003	0.02	0.03	0.08	15
URG Na^+ (0.0–2.5)	0.12	0.001	0.03	0.06	0.17	15
MOUDI Na^+ (0.18–2.5)	0.13	0.012	0.05	0.06	0.24	15
After-filter Na^+ (<0.18)	0.01	0.004	0.01	0.00	0.02	15
PILS Na^+ (0.0–2.5)	0.11	NA	0.04	0.06	0.23	15
MOUDI Coarse Na^+	0.12	0.008	0.05	0.06	0.22	15

filter. Also presented in Table 10 are the geometric mean (d_g) and standard deviation (σ_g) for sulfate and ammonium ion masses. Notice that d_g and σ_g are nearly identical for these two species at about 0.5 and 1.7, respectively, although on an equivalents basis ammonium is in excess by about 20%.

[36] While ammonium and sulfate are generally monomodal, other ion species are not. Interesting features of ions other than ammonium and sulfate are sodium and chloride equivalent concentrations both peaking in the 0.2 μm range, suggesting a fine NaCl mode. Calcium and nitrate covary in the 0.4–0.5 μm range suggesting $Ca(NO_3)_2$, while sodium, calcium, and nitrate all increase in the 1.0–2.0 μm sizes, implying $NaNO_3$ and $Ca(NO_3)_2$, and finally, in the 2.0–10.0 μm range the covariance of nitrate, ammonium, and calcium suggests $Ca(NO_3)_2$ and NH_4NO_3. Usually sodium is also found in the coarse mode, suggesting coarse $NaNO_3$.

[37] Given these general relationships between ion species, three size ranges, 0.3–0.7, 0.7–2.5, and 2.5–10.0 μm, were chosen to approximate the molecular form associated with the measured ion mass concentrations. For the coarse mode, sodium was first associated with chloride and any remaining sodium was then assumed to be in the form of sodium nitrate. The sum of remaining nitrate and sulfate correlates well with ammonium, calcium, and potassium; however, the relative mix of assorted species appears to change from one sampling period to the next. Therefore the mass sum of these ions is combined into a group called remaining mass. Remaining mass would be made up of ammonium sulfate and nitrate, possibly calcium nitrate and sulfate, and potassium sulfate. Similar strategies were used for the 0.7–2.5 μm and 0.3–0.7 μm size ranges. The approximate average molecular make up of these size ranges are summarized in the pie charts presented in Figures 6a, 6b, and 6c.

[38] The aerosol in the fine mode (0.3–0.7 μm) is made up of primarily ammonium sulfate with about 6% ammonium nitrate, 2% sodium chloride, and 9% cations that could not be associated with any measured anions. The analysis of the ionic composition of the URG samples (see discussion in the following section on charge closure) suggests that anion mass might be composed of oxalate. The 0.7–2.5 μm and coarse modes have more compositional structure. The largest mass fraction in this size range is sodium nitrate at about 40% with ammonium sulfate and sodium chloride making up an additional 24%. The remaining fraction is made up of excess cation mass.

5. Charge Closure

[39] Substrates collected with the URG sampling system were analyzed for the anions SO_4^{2-}, NO_3^-, Cl^-, and oxalate, and cations NH_4^+, Na^+, Ca^{2+}, Mg^{2+}, and K^+. Figure 7 is a charge balance scatter plot of all measured cations and anions with and without oxalate. Notice that without the inclusion of oxalate ions there is a clear excess of cations.

[40] Carrying out a charge balance calculation using MOUDI mass size distribution data shows that, on the average, the ratio of cation to anion charge is 1.19, 1.39, and 1.31 in the size ranges of 2.5–10.0 μm, 0.7–2.5 μm, and 0.3–0.7 μm, respectively. The ratio on the order of 1.3 for the 0.3–0.7 μm mode is somewhat higher, but consistent with the cation to anion charge ratio measured using the URG sampling system where it was found that in the size range from 0.0–2.5 μm, the ratio using just the inorganic species was 1.11.

6. Fine Mass Closure

[41] A scatter plot of reconstructed vs. gravimetric fine mass (0.0–2.5 μm) is shown in Figure 8 for two scenarios: (1) the reconstruction equation using a 1.4 multiplier for estimating organic mass from measured organic carbon and based on MOUDI measurements, nitrate interpreted as sodium nitrate:

$$FM = [(NH_4)_2SO_4] + [NaNO_3] + (1.4)[OC] + [EC] + [SOIL] \quad (1)$$

and (2) the same equation but with organic mass interpreted as 1.8[OC]. Nitrate was assumed to be in the form of sodium nitrate because most of the fine (<2.5 μm) nitrate is associated with the fine tail of coarse mode nitrate. The 1.8

Table 6a. Correlation Table of Sodium Mass Concentrations Derived From Various Sampling and Analytic Methodologies

Sodium (0.0–2.5 μm)	URG Na^+	MOUDI Na^+	PILS Na^+
IMPROVE Na	0.91	0.67	0.62
URG Na^+	NA	0.78	0.64
MOUDI Na^+	NA	NA	0.69

Table 7a. Correlation Table of Calcium Mass Concentrations Derived From Various Sampling and Analytic Methodologies

Calcium (0.0–2.5 μm)	URG Ca^{2+}	MOUDI Ca^{2+}	PILS Ca^{2+}
IMPROVE Ca	−0.10	−0.31	0.35
URG Ca^{2+}	NA	0.56	−0.32
MOUDI Ca^{2+}	NA	NA	−0.26

Table 7b. Statistical Summary of Calcium Mass Concentration Derived From Various Sampling and Analytic Methodologies

Variable, $\mu g/m^3$	Mean	UNC	Std Dev	Minimum	Maximum	Valid
IMPROVE Ca (0.0–2.5)	0.02	0.000	0.00	0.02	0.03	25
URG Ca^{2+} (0.0–2.5)	0.03	0.002	0.01	0.01	0.05	25
MOUDI Ca^{2+} (0.18–2.5)	0.02	0.034	0.01	0.01	0.06	25
After-filter Ca^{2+} (<0.18)	0.00	0.002	0.00	0.00	0.01	25
PILS Ca^{2+} (0.0–2.5)	0.04	NA	0.01	0.03	0.07	25
MOUDI Coarse Ca^{2+}	0.02	0.008	0.01	0.01	0.06	25

was derived from an OLS regression with fine mass (FM) as the dependent variable and the various species as independent variables. The R^2 for the scatter plot shown in Figure 8 with the 1.8 multiplier is 0.98, while the slope is 1.05 ± 0.02 and the intercept is not significantly different from zero, implying, to within the uncertainty of the measurements, no bias between reconstructed and gravimetric mass. Using the 1.4 multiplier for calculating organic carbon mass underestimates gravimetric mass by a multiplicative bias of 20%. As shown in Figure 8, at the higher fine mass loadings this bias is greater than the inherent uncertainty of the species concentration measurements.

[42] Figure 8 should be compared to Figure 9 which is the same scatter plot except that R&P organic carbon data with a 1.8 multiplier and averaged to 24 hours are used instead of IMPROVE TOR carbon. For illustrative purposes this scatter plot was created assuming that the R&P measurement had an uncertainty of 5%. Notice that during the lowest concentration time periods (beginning and end of the study period), using R&P carbon measurements to estimate fine mass overestimates gravimetric mass by substantial amounts (more than a factor of 2), while during the time periods of elevated fine mass concentrations, reconstructed fine mass is underestimated. Based on this analysis, it might be concluded that the R&P instrument significantly overestimated carbon mass during some time periods; however, one could make an alternative argument that high vapor pressure carbon volatilized from the IMPROVE channels A (gravimetric mass) and C (carbon mass) at the same rate and that an IMPROVE-type monitoring system inherently underestimates volatile species such as low molecular weight carbon. This issue will be further explored by comparing measured and aerosol-derived fine particle scattering.

[43] Table 11 presents a statistical summary of gravimetric and reconstructed fine mass as well as five major aerosol species contributing to fine mass. Parenthetical values are the percent that each aerosol species contributes to reconstructed fine mass based on TOR-derived carbon and a 1.8 organic carbon multiplier. About 69% of the fine mass is some form of carbonaceous aerosol while ammonium sulfate contributes another 16%. Nitrates, soil, and EC all contribute to fine mass on the order of about 5%.

[44] Table 12 is a similar statistical summary for coarse mass; however, because XRF analysis was not carried out on the PM_{10} filters, soil mass is estimated by differencing coarse mass and the sum of ammonium sulfate, sodium nitrate, OMC, and EC. Then, by inference, about 72% of coarse mass is made up of crustal material while 23% is carbonaceous. Only 4% of coarse mass is associated with inorganic compounds. On the average, the ratio of coarse to fine mass is 0.71; however, in time periods outside the two major OMC episodes, coarse and fine mass have comparable mass concentrations.

Table 8b. Statistical Summary of Potassium Mass Concentration Derived From Various Sampling and Analytic Methodologies

Variable, $\mu g/m^3$	Mean	UNC	Std Dev	Minimum	Maximum	Valid
IMPROVE K (0.0–2.5)	0.06	0.001	0.02	0.03	0.11	25
URG K^+ (0.0–2.5)	0.06	0.001	0.03	0.02	0.13	25
MOUDI K^+ (0.18–2.5)	0.06	0.016	0.03	0.02	0.14	25
After-filter K^+ (<0.18)	0.01	0.006	0.01	0.00	0.03	25
PILS K^+ (0.0–2.5)	0.05	NA	0.02	0.01	0.10	25
MOUDI Coarse K^+	0.05	0.012	0.04	0.01	0.14	25

7. Optical Measurements

[45] The dry ambient nephelometers and transmissometer have effective wavelength sensitivities of 550 nm while the Radiance Research nephelometer wavelength sensitivity is at 530 nm. For Rayleigh scattering the difference between instruments with these two wavelength dependencies is about 14%, while for a typical aerosol the difference would be about 7%. Therefore, for purposes of direct comparison of the Radiance Research nephelometer, used to measuring "dry" scattering, to the Optec instruments which measured ambient scattering, the Radiance Research derived scattering was normalized to the Optec instrument when the relative humidity was less than 30%. Figure 10 presents a temporal plot of total extinction and fine and coarse particle scattering. From Figure 10 it is evident that there are large diurnal changes on many days and that scattering-extinction is near Rayleigh during some time periods and as high as 200+ Mm^{-1} on other days. During the first week and last days of the study the atmosphere was near Rayleigh scattering, while Julian days 225–234 characterize an episode where scattering-extinction was elevated. It is also evident from Figure 10 that the largest contribution to extinction is scattering by particles less than 2.5 μm.

Table 8a. Correlation Table of Potassium Mass Concentrations Derived From Various Sampling and Analytic Methodologies

Potassium (0.0–2.5) μm)	URG K^+	MOUDI K^+	PILS K^+
IMPROVE K	0.97	0.55	0.91
URG K^+	NA	0.52	0.90
MOUDI K^+	NA	NA	0.57

Table 9a. Correlation Table of Carbon and EC (Black Carbon) Mass Concentrations Derived From Various Sampling and Analytic Methodologies

Carbon (0.0–2.5 μm)	R&P TC	IMPROVE TOR EC	Aethalometer BC
IMPROVE TOR TC	0.89	0.91	0.94
R&P TC	NA	0.80	0.91
IMPROVE TOR EC	NA	NA	0.87

Table 9b. Statistical Summary of Carbon Mass Concentration Derived From Various Sampling and Analytic Methodologies

Variable, $\mu g/m^3$	Mean	UNC	Std Dev	Minimum	Maximum	Valid
IMPROVE TOR TC (0.0–2.5)	4.09	0.081	2.75	0.80	12.57	49
R&P TC (0.0–2.5)	5.46	NA	1.78	3.05	10.20	49
IMPROVE TOR EC (0.0–2.5)	0.39	0.014	0.22	0.10	1.23	49
Aethalometer BC (0.0–2.5)	0.29	0.013	0.13	0.13	0.68	49
IMPROVE Coarse TOR TC	0.99	0.080	0.32	0.46	1.81	49
IMPROVE Coarse TOR EC	0.04	0.014	0.11	−0.37	0.28	49

[46] Table 13 further summarizes the optical parameters. The difference between average dry and ambient scattering is only on the order of about 2.63 Mm^{-1}, which is well within the uncertainty of the measurements. This small difference is consistent with the low average relative humidity and little hygroscopic growth at ambient humidities. Furthermore, the difference between PM_{10} and $PM_{2.5}$ scattering is small at 1.46 Mm^{-1}, which again is within the nephelometers' stated uncertainties. It is known that the PM_{10} nephelometer underestimates coarse particle scattering by about a factor of 2; therefore average coarse particle scattering is about 3 Mm^{-1}. This is consistent with the average gravimetric coarse mass of 7.46 $\mu g/m^3$. Assuming a mass scattering efficiency of 0.6 m^2/g, 7.46 $\mu g/m^3$ corresponds to 4.48 Mm^{-1}. Differencing total extinction and measured PM scattering, plus 1.5 Mm^{-1} to account for nephelometer large particle truncation error, yields 9.7 Mm^{-1} of absorption. Therefore, based on optical measurements, 75% of extinction is dry fine particle scattering, 6% is coarse particle scattering, 14% is coarse and fine absorption, and 5% is scattering due to absorbed water.

8. Dry Fine Particle Scattering Closure

[47] In this section, closure between measured fine particle scattering and fine particle scattering estimated from measured aerosol mass concentrations will be explored. The objectives of carrying out these calculations are twofold in that both the ability to estimate aerosol optical properties and the accuracy of aerosol measurements can be assessed. Of interest is further examination of the discrepancy between carbonaceous concentrations derived from R&P semi-continuous measurement and the 24-hour bulk TOR carbon technique. It was shown that excellent closure was achieved between 24-hour gravimetric mass and the sum of individual aerosol species when the 24-hour TOR analysis was used to estimated carbon concentrations, but there was poor agreement when R&P-derived carbon was used.

[48] Estimating the uncertainty associated with mass scattering efficiencies is difficult because of assumptions required to make the efficiency calculation. Typically, either a completely external or internal mixing state is assumed, when in reality scanning electron microscope data clearly suggests that a variety of mixing states exist [*Hand et al.*, 2004]. Furthermore, the mixed states may or may not be uniform and some particles may have inclusions such as chain aggregates of carbon that are typically associated with diesel emissions. *Fuller et al.* [1999] have shown that the extinction characteristics of particles with absorbing inclusions can vary significantly depending on the internal geometry of the absorbing particles.

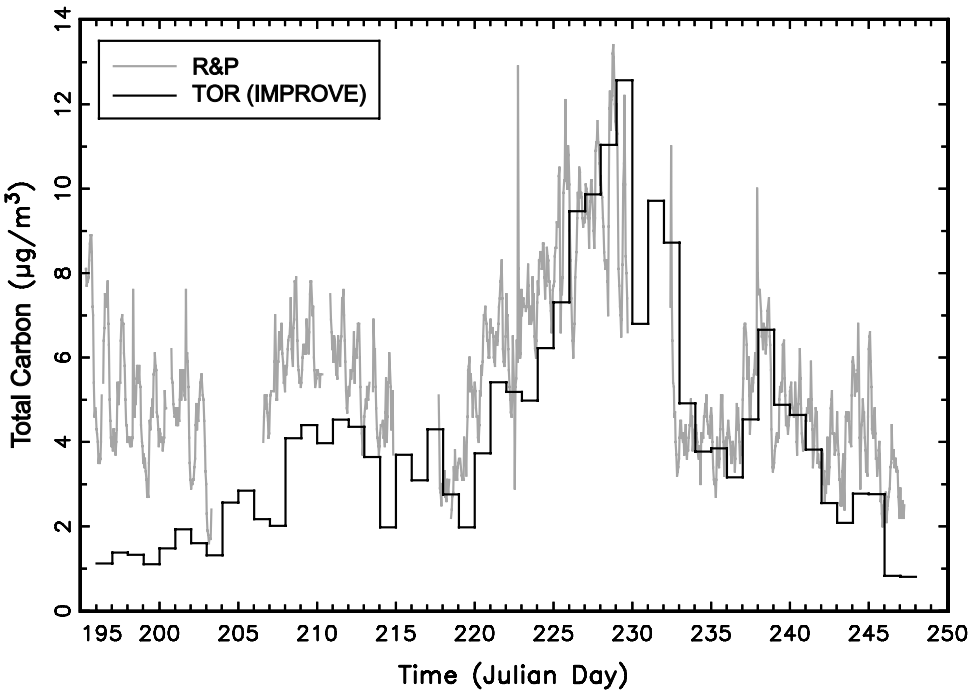

Figure 4a. Temporal plot of semi-continuous fine total carbon mass concentration derived from the R&P and IMPROVE TOR systems.

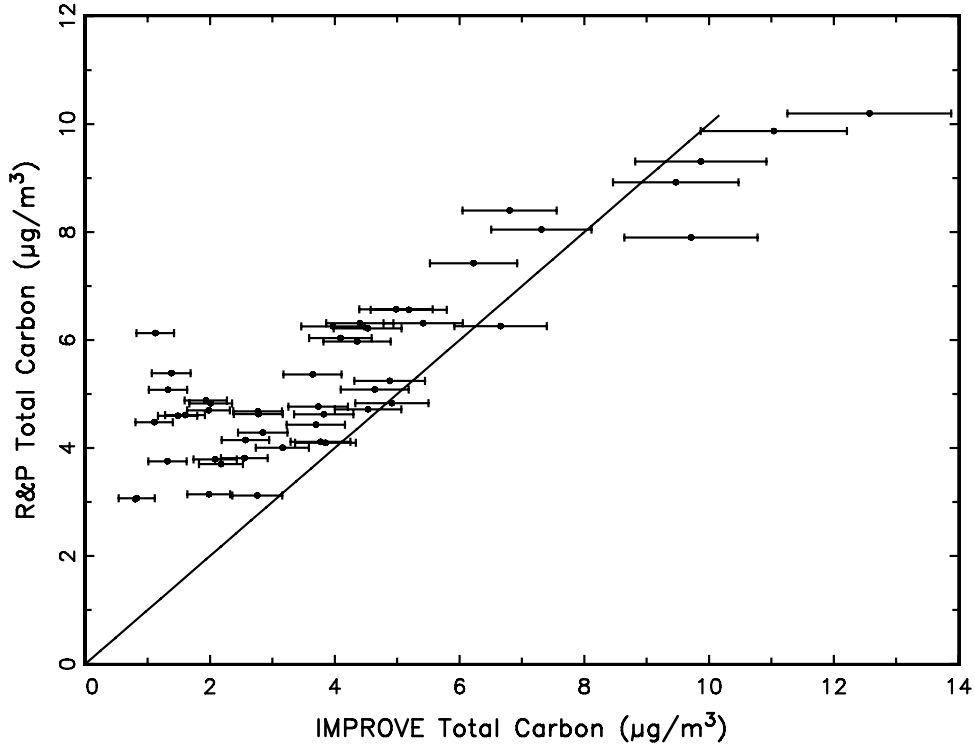

Figure 4b. Scatter plot of IMPROVE and R&P fine total carbon mass concentrations. R&P data have been averaged to 24 hours for comparison to IMPROVE data.

[49] Therefore, because the uncertainty of scattering measurements can be approximated by the introduction of standard gases into the nephelometers, scattering measurements will be used to estimate the combined uncertainty of the aerosol measurements themselves and the uncertainty associated with assumptions required to carry out the aerosol optical property calculations.

[50] Two models will be considered: first, a simple model assuming external mixing assumptions with constant mass scattering coefficients and constant aerosols types [*Malm et al.*, 1994, 2000]:

$$b_{sf} = (3)\left[(NH_4)_2SO_4\right] + (1)[NaNO_3] + (4)[OMC] + (1)[SOIL] \quad (2)$$

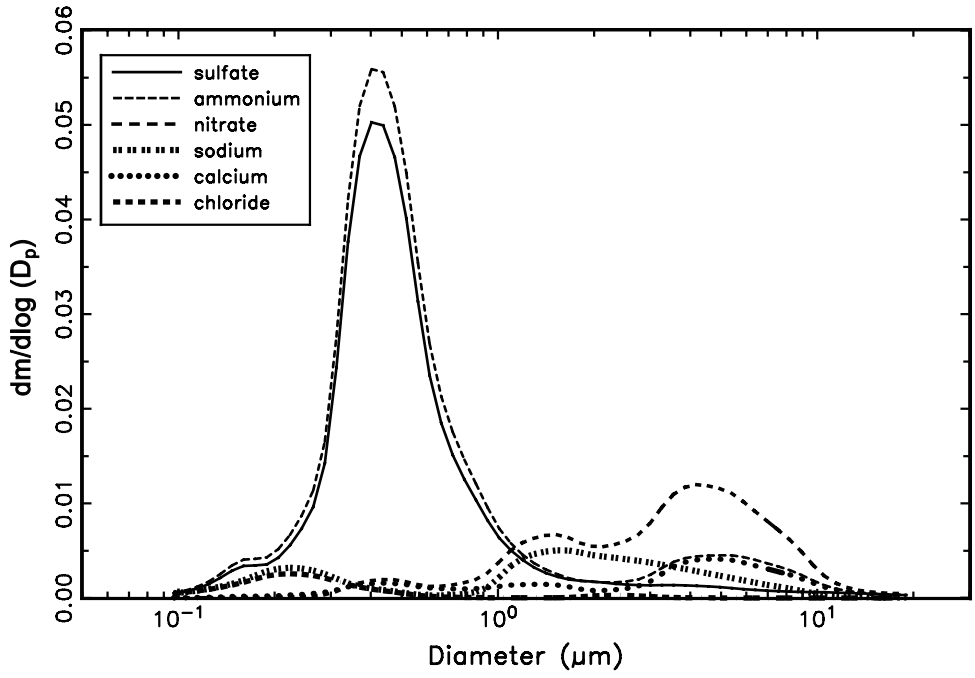

Figure 5. Equivalent mass size distribution of selected ions on Julian day 243 (31 August).

Table 10. Statistical Summary of Ammonium and Sulfate Mass Concentration, Geometric Mass Mean Diameter, and Geometric Standard Deviation

Variable	Mean	Std Dev	Minimum	Maximum	Valid
		Sulfate			
MASS, $\mu g/m^3$	0.82	0.16	0.03	1.08	34
After-filter, $\mu g/m^3$	0.30	0.28	0.08	0.83	34
d_g, μm	0.48	0.04	0.00	0.53	34
σ_g	1.69	0.09	0.01	1.87	34
		Ammonium			
MASS, $\mu g/m^3$	0.37	0.09	0.20	0.56	34
After-filter, $\mu g/m^3$	0.17	0.14	0.04	0.46	34
d_g, μm	0.46	0.04	0.38	0.51	34
σ_g	1.65	0.07	1.53	1.85	34

and second, a model with a combination of external and internal mixing assumptions and with varying mass scattering efficiencies as determined from differential mobility analyzer (DMA) number size distribution measurements:

$$b_{sf} = (e_f)\left([(NH_4)_2SO_4] + [OMC] + [EC]\right) + (1)[NaNO_3] + (1)[SOIL] \quad (3)$$

[51] In equation (2), the coefficients 3.0, 1.0, 4.0, and 1.0 are the average mass scattering efficiencies in m^2/g associated with each species, while in equation (3), e_f are DMA-derived mass scattering efficiencies that are based on Mie theory calculations and on volume-weighted indices of refractions and mass densities which implicitly assume uniform mixtures of sulfate and carbonaceous material. In all cases a 1.8 multiplier was used to estimate organic carbon mass from measured organic carbon. With the addition of an *f*(RH) term to account for aerosol growth, equation (2) is similar to the equation used by the EPA regional haze program [*U.S. Environmental Protection Agency*, 2003] to estimate scattering for tracking progress toward natural visibility conditions, the difference being the tracking progress guidance equation assumes nitrate to be in the form of ammonium nitrate.

[52] The differential mobility analyzer was used to size particles every 15 minutes over size ranges of 0.038–0.8 μm in 25 steps. Figure 11 shows two representative derived mass size distributions assuming a density of 1.4 g/cm^3. Early in the study, around Julian day 215, the mass size distributions showed clear multimodal characteristics, while later in the study during the episode having relatively high carbonaceous mass concentrations, the peak concentrations associated with the mass size distributions were centered at about 0.35 μm and were relatively narrow with σ_g equal to about 1.5. Table 14 summarizes d_g and σ_g as well as derived mass and mass scattering efficiencies, e_f, for 814 measurements. Mass scattering efficiencies were calculated using Mie theory for spherical particles and assuming, consistent with measured inorganic mass size distributions, that the size mode from 0.1–1.0 μm contained only ammonium sulfate and carbonaceous mass whose relative concentrations were estimated from the URG and IMPROVE 24-hour measurements.

[53] The index of refraction for "soot" or elemental carbon as reported in the literature [*Fuller et al.*, 1999] varies from 1.25+i0.25 to 2.0+i1.0. For these calculations an elemental carbon index of refraction of 1.8–i0.5 as reported by *Twitty and Weinman* [1971] was used. Therefore the volume-weighted index of refraction for the internally mixed state was estimated assuming 1.55, 1.53, and 1.8+i0.5 as the indices of refraction for ammonium sulfate, and organic and elemental carbon, respectively, while volume-weighted densities were calculated assuming 1.78 g/cm^3, 1.4 g/cm^3, and 1.8 g/cm^3 for these species. Nitrate was, based on the MOUDI inorganic mass size distribution, assumed to be in the form of sodium nitrate and to have an efficiency consistent with it being the "tail" of the coarse particle mode [*Malm et al.*, 2003].

[54] Figure 12 shows a plot of mass scattering efficiency of the 0.1–1.0 μm internally mixed mode as a function of time. One of the greatest uncertainties in the estimate of mass scattering efficiency is the unknown optical characteristics of elemental carbon. For instance, the reported range of the imaginary component of the index of refraction for elemental carbon is from a low of 0.25 to a maximum of 1.0, which by itself will result in about a 10% uncertainty in the calculated mass scattering efficiency of the internally mixed aerosol, resulting in a commensurate uncertainty in estimated scattering.

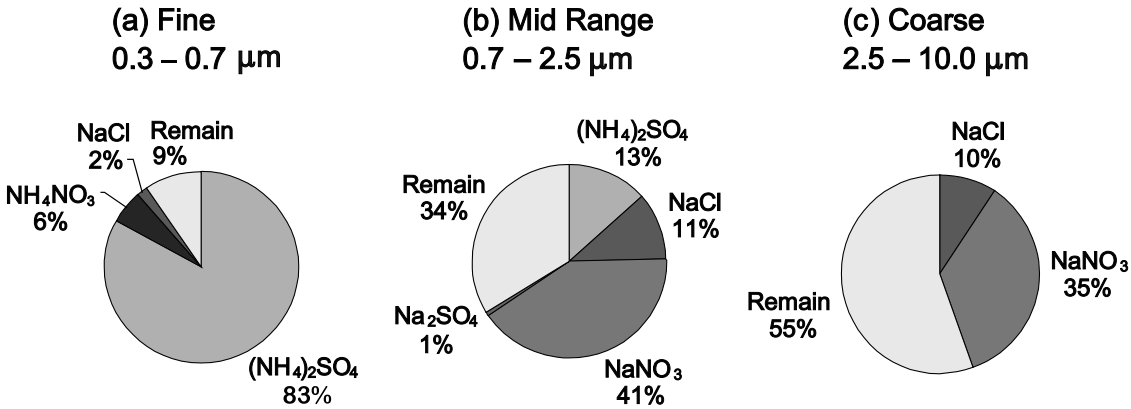

Figure 6. Average composition (N = 25) of aerosol mass concentration for size ranges of 0.3–0.7, 0.7–2.5, and 2.5–10.0 μm.

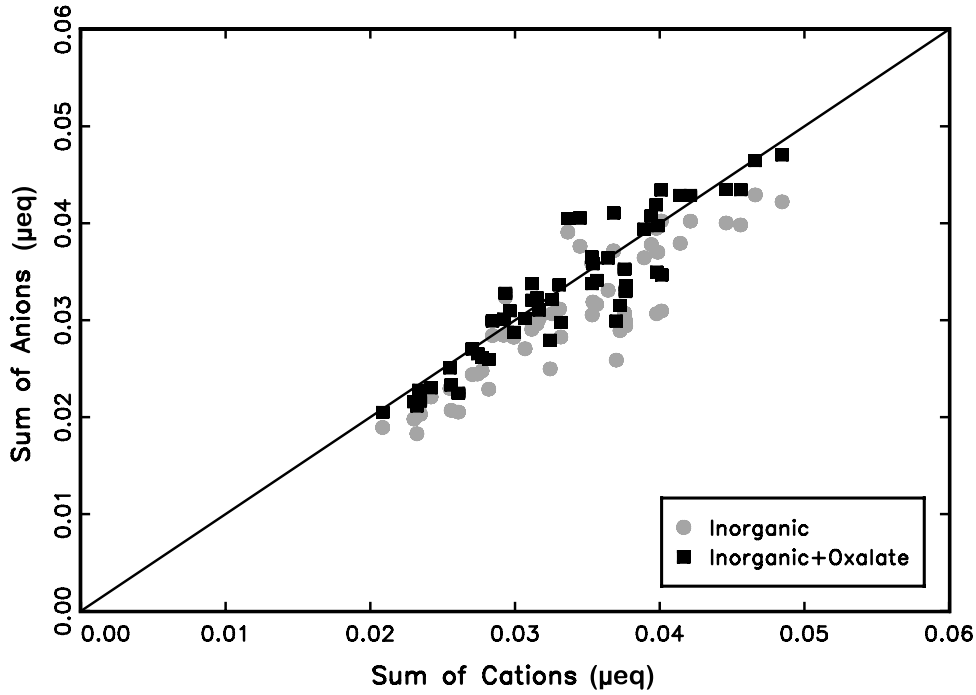

Figure 7. Charge balance between cations and anions with and without oxalate included.

[55] Notice that the mass scattering efficiencies vary from a low of almost 2 m^2/g to a maximum of 5.7 m^2/g. This graph should be compared to Figure 1 where species concentrations are plotted as a function of time. Generally, the time periods of highest mass scattering efficiency occur during those time periods when carbonaceous material and fine mass are elevated. During the episode surrounding Julian day 230, carbonaceous material is 80–90% of measured fine mass, implying that during this time period organic carbon mass scattering efficiencies are about 1.5 times greater than the usually assumed 4.0 m^2/g [*U.S. Environmental Protection Agency*, 1999].

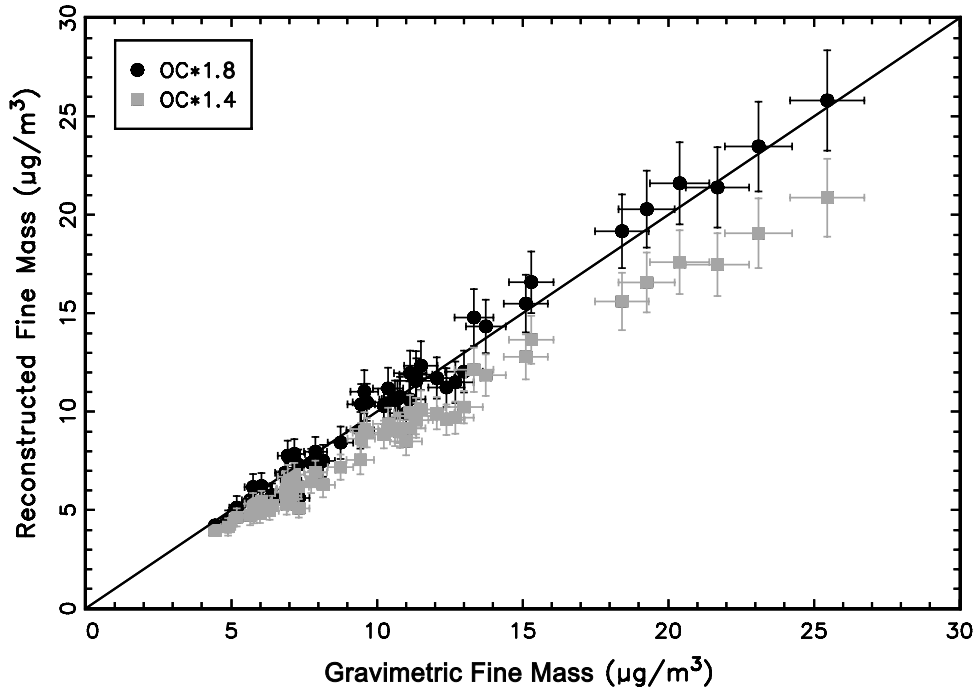

Figure 8. Scatter plot of gravimetric fine mass and the sum of derived aerosol species mass or reconstructed fine mass concentrations with 1.4*OC (gray) and 1.8*OC (black).

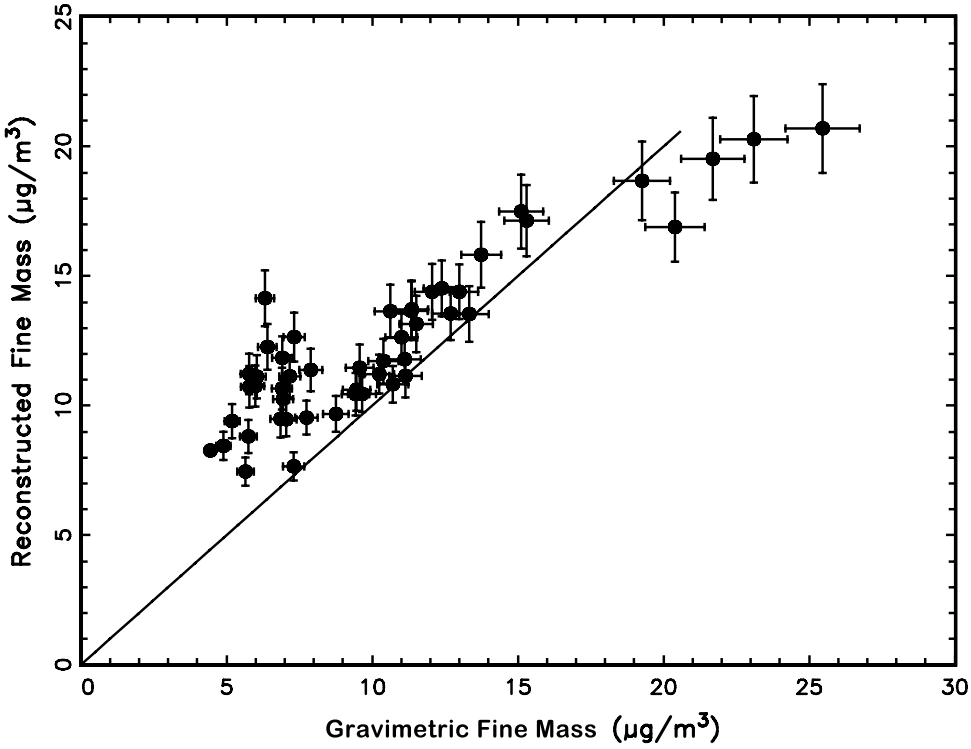

Figure 9. Scatter plot of gravimetric fine mass and sum of derived aerosol species mass or reconstructed fine mass concentrations with R&P carbon times 1.8 and with an assumed uncertainty of 5%.

[56] One-hour dry aerosol scattering was calculated using the semi-continuous PILS inorganic and R&P carbon data with and without normalizing to 24-hour average bulk aerosol data. Figure 13 is a scatter plot of dry measured and aerosol scattering assuming constant mass scattering efficiencies (equation (2)) and calculated mass scattering efficiencies based on DMA size distribution measurements (equation (3)). Error bars are not included for reconstructed aerosol scattering because of unknown uncertainties inherent in the scattering calculation. In both cases R&P-derived carbon mass concentrations normalized to 24-hour average IMPROVE TOR carbon were used. Notice that aerosol scattering using the assumption of a constant mass scattering efficiency of 4.0 m^2/g for organic and 3.0 m^2/g for sulfate mass agrees quite well with measured scattering in those time periods where scattering is below about 60 Mm^{-1} which is before and after the elevated organic mass episode. During elevated organic aerosol concentration periods (JD = 225–235), scattering was under-predicted by as much as 30%. The internally mixed variable mass scattering model with its various assumptions yields, on the average, an unbiased estimate of measured scattering. An OLS regression between measured and modeled scattering yields an $R^2 = 0.91$, a slope of 0.98 ± 0.012, and an intercept term that is not statistically different from 0.0. However, during the first smoke episode, aerosol scattering is systematically overestimated, while during the second and larger smoke episode, aerosol scattering is underestimated, possibly reflecting different mixing characteristics or aerosol morphology.

[57] Figure 14 is a scatter plot of dry measured and aerosol scattering using R&P carbon without normalizing to the 24-hour bulk TOR carbon measurements. Compar-

Table 11. Statistical Summary of $PM_{2.5}$ Gravimetric and Reconstructed Mass (Recon FM) and the Mass Associated With the Main Aerosol Species Types (Shown Parenthetically is the Percentage That Each Aerosol Type Contributes to Reconstructed Fine Mass)

Variable, μg/m³	Mean	UNC	Std Dev	Minimum	Maximum	Valid
Fine Mass	9.61	0.08	4.47	4.06	23.35	52
Recon FM (1.4*OC)	8.35	0.11	3.73	3.85	19.32	52
Recon FM (1.8*OC)	9.85	0.14	4.74	4.09	23.86	52
Ammonium Sulfate	1.59 (16.1)	0.007	0.41	0.84	2.38	52
Sodium Nitrate	0.48 (4.9)	0.013	0.23	0.16	1.20	52
OMC(1.4*OC)	5.30	0.11	3.57	0.84	15.87	52
OMC(1.8*OC)	6.81 (69.1)	0.14	4.59	1.08	20.41	52
EC	0.38 (3.8)	0.014	0.22	0.10	1.23	52
SOIL	0.59 (6.0)	0.006	0.16	0.29	0.94	52

Table 12. Statistical Summary for the Coarse Mass Fraction (2.5–10.0 μm)

Variable, μg/m³	Mean	UNC	Std Dev	Minimum	Maximum	Valid
Coarse Mass	7.46	0.10	2.19	4.28	14.41	52
Ammonium Sulfate	0.00	0.01	0.06	−0.20	0.17	52
Sodium Nitrate	0.32	0.005	0.24	−0.11	1.48	52
OMC	1.73	0.080	0.57	0.83	3.26	52
EC	0.04	0.014	0.11	−0.37	0.28	52
SOIL (estimated)	5.38	NA	2.05	1.29	11.63	52

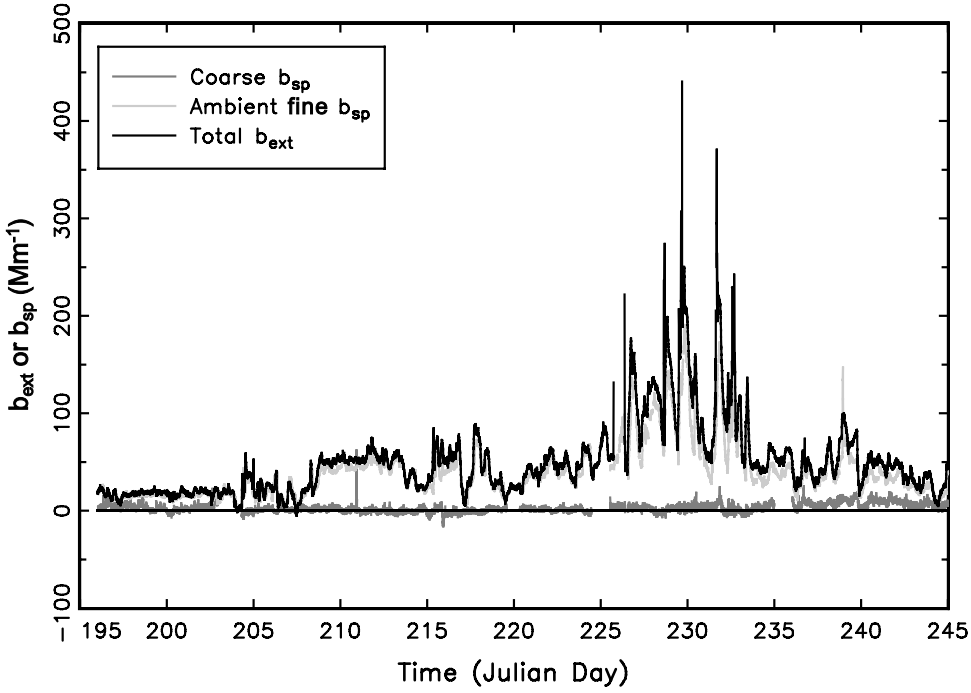

Figure 10. Temporal plot of extinction and fine and coarse particle scattering.

ing this figure to Figure 9, a scatter plot of reconstructed vs. gravimetric fine mass, shows the same bias at low and high scattering. Aerosol scattering is overestimated by almost 100% at low scattering values while at higher scattering values aerosol scattering is underestimated by about 25%. The over- and underestimation is apparently related to the R&P carbon measurement uncertainty or imprecision.

[58] As discussed previously, it is difficult to explicitly assign uncertainty to theoretically estimated scattering given the varied assumptions associated with the optical (Mie theory) and physical properties and the inherent measurement uncertainty of the semi-continuous measurements. However, an estimate of the uncertainty of reconstructed scattering can be achieved by assuming measured scattering as a reference value. The mean and standard deviation of the difference and absolute value of the difference between measured and aerosol scattering is presented in Table 15 and a temporal plot of the difference is presented in Figure 15 along with measured scattering divided by five (to keep graphs on comparable scales). Notice that on the average the mean difference between these two parameters is only 0.75 Mm^{-1} or about 2%. However, the mean of the absolute value of the difference is almost 7 Mm^{-1} while the standard deviation of the mean difference is about 9.0 Mm^{-1}. Therefore a reasonable estimate of hourly aerosol scattering uncertainty, defined as one standard deviation of the mean difference, is $\bar{b}_{sp} \pm 9.0$ Mm^{-1} compared to about ± 2.0 Mm^{-1} for measured scattering. However, Table 15 shows that the differences can approach $\pm 30-40$ Mm^{-1}.

[59] A similar analysis using the bulk 24-hour data shows that the mean of the absolute difference between estimated and measured scattering is small, on the order of a few percent, implying the variability between observed and estimated scattering lies in the uncertainty of the near real time aerosol measurements. A convincing argument can be made that much of the uncertainty in reconstructed scattering is linked to uncertainty in the R&P carbon measurement. Figure 15 shows that the differences between measured and reconstructed scattering have strong diurnal characteristics that match the diurnal pattern of measured scattering. The greatest difference between measured and reconstructed scattering corresponds to the highest levels of scattering and, conversely, the lowest differences are commensurate with lowest scattering values. From Figure 15 it is also evident that the differences fluctuate around zero, showing that there is almost a zero additive bias on the average as indicated by the near zero mean difference between measured and aerosol scattering values. A cursory examination of Figure 15 seems to suggest that as scattering or aerosol concentration increases, the diurnal bias increases. However, as the ratio of inorganic to organic scattering increases, the diurnal bias approaches zero and vice versa; when that ratio is small (<0.1-high organic mass), the diurnal bias reaches its maximum. This implies that the R&P carbon measurement is not only

Table 13. Statistical Summary of Relative Humidity, PM_{10}, $PM_{2.5}$ Ambient and Dry Scattering, and Total Extinction

Variable, Mm^{-1}	Mean	Std Dev	Minimum	Maximum	Valid
RH	33.51	10.62	9.25	82.40	5606
b_{sp}_10	41.37	28.91	6.06	192.83	5606
$b_{sp}\_2.5$	39.91	28.86	5.58	190.69	5606
b_{sp}_dry	37.28	28.99	5.23	189.85	5606
b_{ext}	49.60	39.78	3.83	448.00	5606

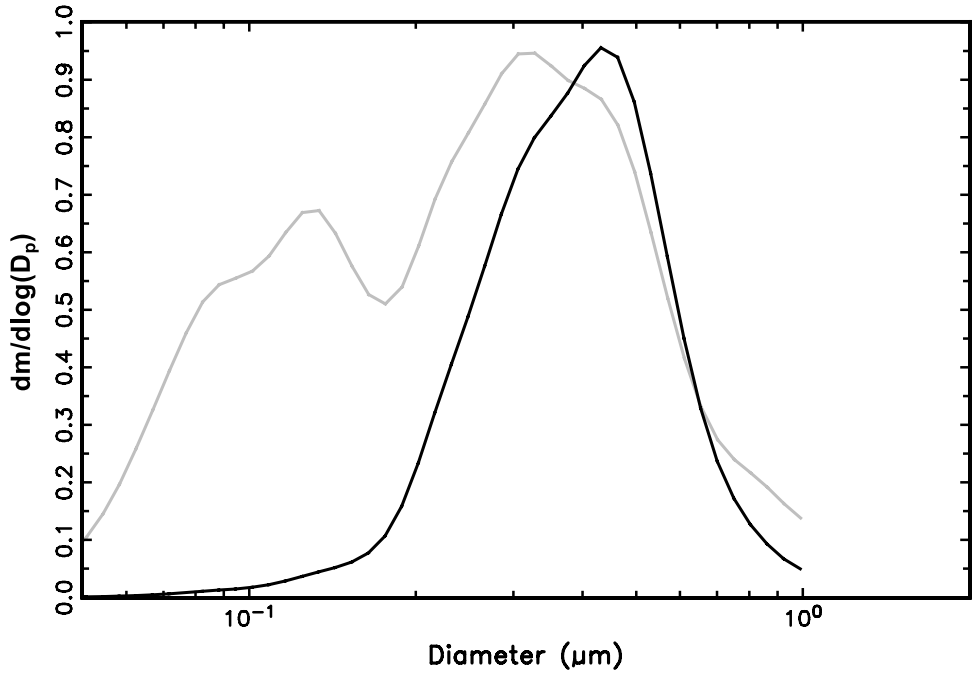

Figure 11. Representative aerosol mass size distributions for Julian days 215 (gray) and 230 (black).

biased high or low on the average over extended time periods, but also, even though it reflects some diurnal variability in carbonaceous material, the measurement is underestimating the true diurnal signature by as much as 40–50%.

[60] Table 16 summarizes the measured and aerosol scattering based on equation (3) as well as the approximate amount of scattering attributed to each aerosol species. Measured and aerosol scattering are within 2% of each other. Organics on the average account for 83.5% of scattering, while sulfate aerosol is a distant second at 12.7%.

9. Summary

[61] The primary objectives of the study were to characterize the physical, chemical, and optical properties of a carbon-dominated aerosol with an eye toward a better characterization of the ratio of organic carbon to total organic carbon compound weight and the organic mass scattering efficiencies. A secondary objective was to evaluate the comparability of a wide variety of aerosol monitoring systems including two semi-continuous monitors measuring inorganic ions and total carbon.

[62] During this time period the average gravimetric mass concentration was 10.48 $\mu g/m^3$ with organics, elemental carbon, ammonium sulfate, and sodium nitrate making up 70.6, 4.0, 15.1, and 4.6%, respectively. However, during one large smoke episode carbonaceous material exceeded 80% of the fine mass for 14 days when the fine mass concentrations were 15–20 $\mu g/m^3$.

[63] The 24-hour ''bulk'' measurements of various aerosol species compared more favorably with each other than with the semi-continuous data. Sulfates, more than any other species, compared the most favorably across all monitoring systems. The difference between the two sampling systems for sulfate was 8% with an intervariable correlation coefficient of 0.98, while sulfate derived from the MOUDI sampler was 6% lower than the average of IMPROVE and URG. Sulfate derived from the PILS system was averaged to 24 hours. On the average, PILS sulfate compared favorably to URG and IMPROVE sulfate, although the intervariable correlation was lower at 0.7 and PILS sulfate was additively biased low at about 0.15 $\mu g/m^3$.

[64] The difference between URG and IMPROVE nitrates was on the order of 18% but with a high intervariable correlation coefficient of 0.98. A regression between the two data sets showed both a multiplicative and additive bias. MOUDI nitrate was 50% lower than the average of IMPROVE and URG nitrate while PILS nitrate was 22% lower than the URG/IMPROVE average. PILS nitrate was both additively and multiplicatively biased low. Intervariable correlation for nitrate among all systems was about 0.78 or better.

[65] URG- and MOUDI-measured ammonium also compared quite favorably with an 8% difference and an

Table 14. Statistical Summary of Geometric Mass Mean Diameter, Geometric Standard Deviation, Estimated Mass Between 0.1–1.0 μm, and Calculated Mass Scattering Coefficient All Derived From DMA Data

Variable	Mean	Std Dev	Minimum	Maximum	Valid
Estimated Mass, $\mu g/m^3$	7.95	4.39	1.29	28.83	814
Real Index of Refraction	1.56	0.01	1.55	1.59	814
Imaginary Index Refraction	0.02	0.01	0.01	0.04	814
d_g, μm	0.30	0.04	0.22	0.41	814
σ_g	1.71	0.11	1.48	2.06	814
e_f, m^2/g	4.21	0.74	2.11	5.67	814

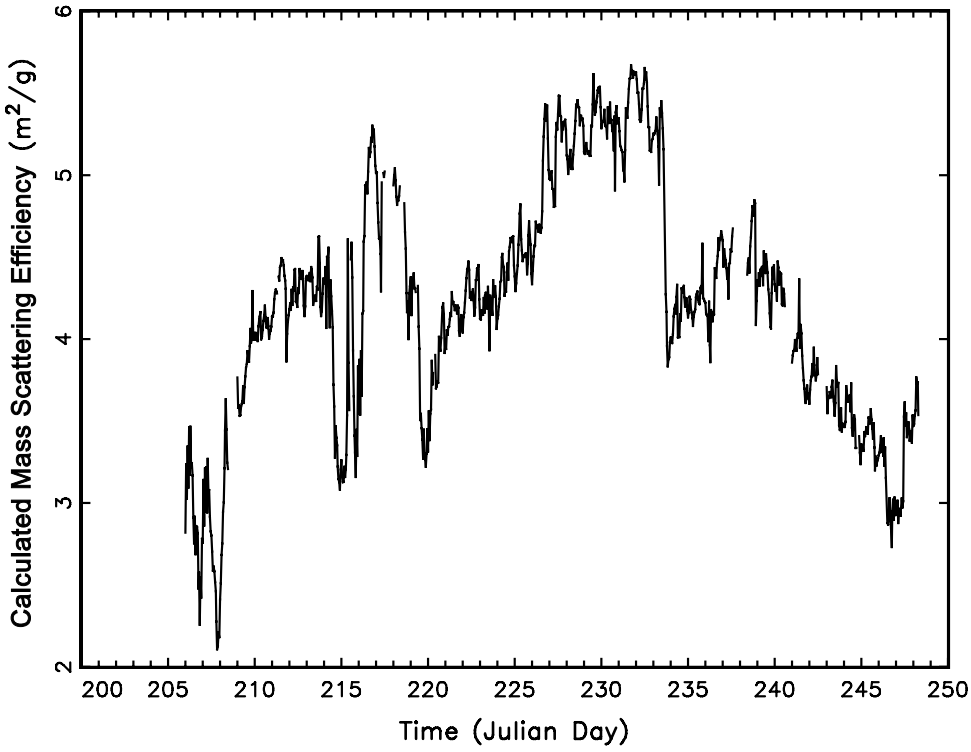

Figure 12. Temporal plot of the calculated mass scattering efficiencies derived from DMA data.

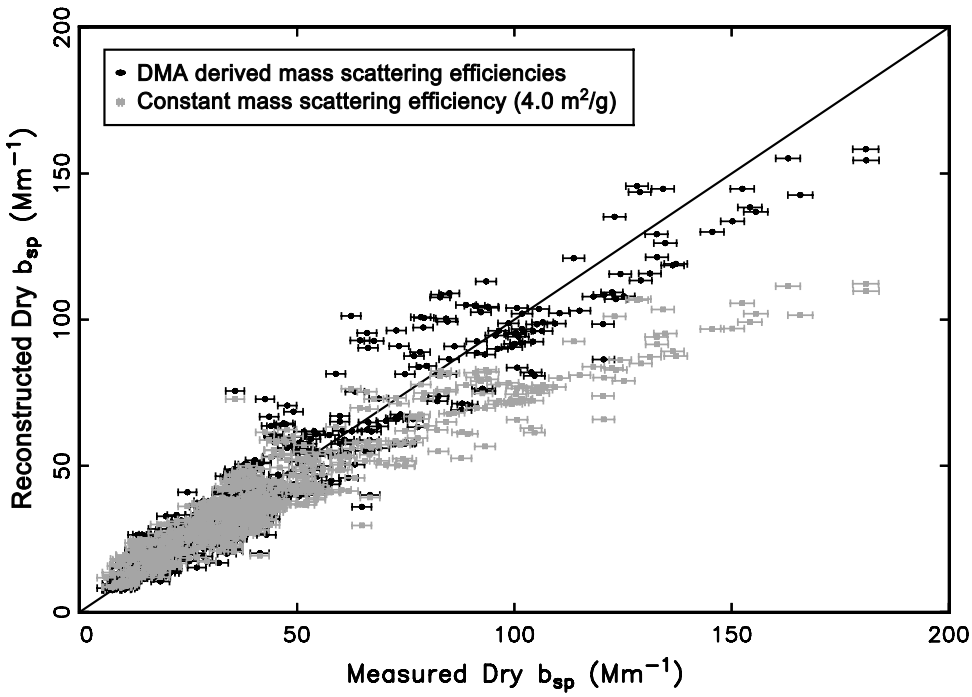

Figure 13. Scatter plot of calculated aerosol versus measured dry scattering assuming a constant 4.0 m^2/g and 3.0 m^2/g for organic carbon and sulfate mass scattering efficiencies, respectively, and the DMA-derived mass scattering efficiencies shown in Figure 12.

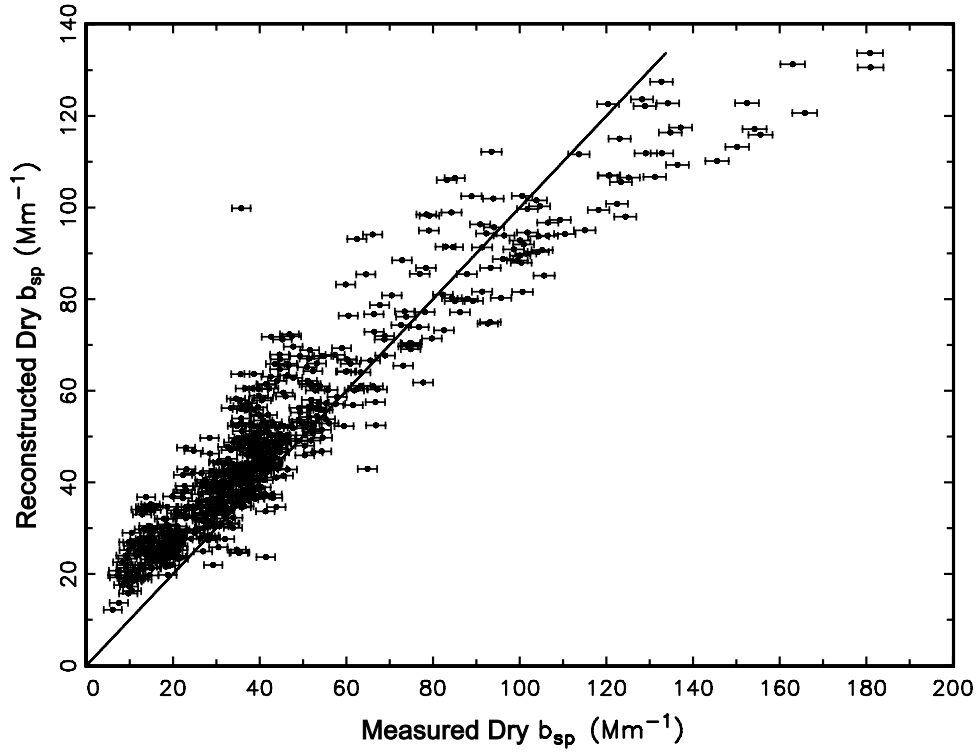

Figure 14. Scatter plot of reconstructed versus measured scattering assuming DMA-derived mass concentrations with 1.8*R&P organic carbon concentrations.

Table 15. Statistical Summary of the Difference and Absolute Value of the Difference Between Measured and Aerosol Scattering for 1-Hour Time Periods

Variable, Mm^{-1}	Mean	St dev	Minimum	Maximum	Valid
$b_{sp} - b_{sp,aerosl}$	0.75	9.03	−39.85	34.16	661
($\|b_{sp} - b_{sp,aerosl}\|$)	6.84	5.95	0.00	39.85	661

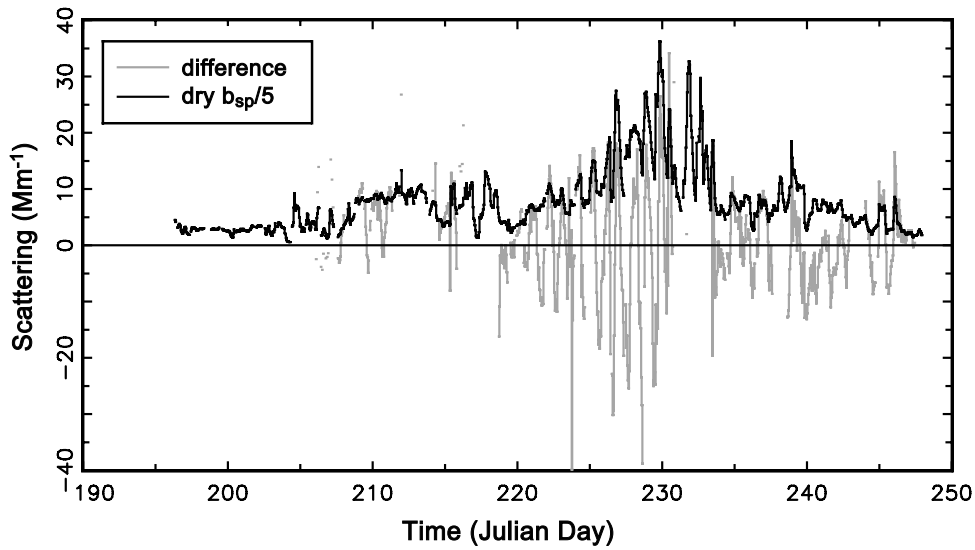

Figure 15. Temporal plot of measured scattering divided by five (black) and the difference between measured and aerosol scattering.

Table 16. Statistical Summary of Measured Scattering, Reconstructed Aerosol Scattering, and the Scattering Associated With Various Aerosol Species (Parenthetical Values Are the Approximate Percentage Contribution of Each Aerosol Species to Reconstructed Scattering)

Variable, Mm^{-1}	Mean	Std Dev	Minimum	Maximum	Valid
$b_{sp,measured}$	43.02	29.01	7.48	158.29	661
$b_{sp,aerosol}$	43.77	29.93	6.07	180.97	661
Ammonium Sulfate	5.54 (12.7)	2.38	1.86	13.98	661
Sodium Nitrate	0.34 (0.8)	0.29	0.04	2.41	661
OMC	36.53 (83.5)	28.34	2.27	152.39	661
SOIL	0.62 (1.4)	0.17	0.29	0.94	661

intervariable correlation of 0.93. Likewise, potassium as measured by the different systems compared well even though K from the IMPROVE system was estimated using XRF while for the other systems the analytic technique was ion chromatography. As with sulfate and nitrate, PILS K^+ is additively biased low at about 0.01 $\mu g/m^3$ or about 17% on the average. All other measured ionic species compare less favorably, primarily because concentrations are low and near the minimum detectable level.

[66] On the average, R&P-derived TC was about 33% higher than IMPROVE TOR TC, but more importantly, there was not a clear additive or multiplicative bias between the two measurements. Generally, when TC was low, R&P TC was greater than IMPROVE TOR, while the opposite was true at higher concentrations. Closure calculations between mass reconstructed from aerosol species and gravimetric mass on the one hand and dry reconstructed and measured scattering on the other strongly suggested that R&P carbon measurements were in error and the error was related to ambient levels of carbonaceous material. This bias not only showed up over the longer time frame of weeks but also on a diurnal basis. Expressed as the average of the absolute value of the mean difference, the estimated average uncertainty of the R&P OC concentrations is about 0.9 $\mu g/m^3$ for an average OC mass concentration of 2.1 $\mu g/m^3$, or about a 43% uncertainty.

[67] Fine mass closure calculations also showed that the factor for estimating organic mass concentrations from measurements of organic carbon for this study was about 1.8 rather than the more typically used 1.4. Furthermore, fine scattering closure calculations clearly showed that the use of 4.0 m^2/g for fine organic mass scattering coefficients was an underestimate by at least 30% for periods with high organic mass concentrations. This was verified by estimating mass scattering coefficients from DMA number size distribution measurements. Even though the average mass scattering coefficient was near 4 m^2/g, during the smoke episodes the mass scattering efficiencies were as high as about 5.7 m^2/g. The EPA regional haze guidance for tracking progress toward achieving the national visibility goal suggests the use of 1.4 as the factor for estimating organic mass from organic carbon measurements and a 4.0 m^2/g mass scattering efficiency for estimating the scattering associated with organic mass. These two factors combine to yield an underestimate of smoke-related scattering by about a factor of two if the results of this analysis are universally true. These results should be reexamined for other smoke events where aerosol aging and fuel types are different.

[68] **Acknowledgment.** The assumptions, findings, conclusions, judgments, and views presented herein are those of the authors and should not be interpreted as necessarily representing the National Park Service policies.

References

Armendariz, A. J., and D. Leith (2002), Concentration measurement and counting efficiency for the aerodynamic particle sizer 3320, *J. Aerosol Sci.*, *33*, 133–148.

Bench, G., and P. Herckes (2004), Measurement of contemporary and fossil carbon contents of PM2.5 aerosols: Results from Turtleback Dome, Yosemite National Park, *Environ. Sci. Technol.*, *38*, 2424–2427.

Bench, G., P. G. Grant, D. Ueda, S. S. Cliff, K. D. Perry, and T. A. Cahill (2001), The use of STIM and PESA to respectively measure profiles of aerosol mass and hydrogen content across Mylar rotating drum impactor samples, *Aerosol Sci. Technol.*, *36*, 642–651.

Brown, S. G., P. Herckes, L. Ashbaugh, M. P. Hannigan, S. M. Kreidenweis, and J. L. Collett Jr. (2002), Characterization of organic aerosol present in Big Bend National Park, Texas during the Big Bend Regional Aerosol and Visibility Observational (BRAVO) study, *Atmos. Environ.*, *36*, 5807–5818.

Carrico, C. M., S. M. Kreidenweis, J. L. Collett Jr., and W. C. Malm (2005), Hygroscopic growth behavior of a carbon dominated aerosol in Yosemite National Park, *Atmos. Environ.*, *39*(8), 1393–1404.

Chow, J. C., J. G. Watson, L. C. Pritchett, W. R. Pierson, C. A. Frazier, and R. G. Purcell (1993), The DRI thermal/optical reflectance carbon analysis system: Description, evaluation, and applications in U. S. air quality studies, *Atmos. Environ., Part A*, *27*(8), 1185–1201.

Day, D. E., and W. C. Malm (2001), Aerosol light scattering measurements as a function of relative humidity: A comparison between measurements made at three different sites, *Atmos. Environ.*, *35*, 5169–5176.

Dick, W. D., P. Saxena, and P. H. McMurry (2000), Estimation of water uptake by organic compounds in submicron aerosols measured during the Southeastern Aerosol and Visibility Study, *J. Geophys. Res.*, *105*(D1), 1471–1479.

Fuller, K. A., W. C. Malm, and S. M. Kreidenweis (1999), Effects of mixing on extinction by carbonaceous particles, *J. Geophys. Res.*, *104*, 15,941–15,954.

Hand, J. L., and S. M. Kreidenweis (2002), A new method for retrieving particle refractive index and effective density from aerosol size distribution data, *Aerosol Sci. Technol.*, *36*, 1012–1026.

Hand, J. L., S. M. Kreidenweis, D. E. Sherman, J. L. Collett Jr., S. V. Hering, D. E. Day, and W. C. Malm (2002), Aerosol size distributions and visibility estimates during the Big Bend Regional Aerosol Visibility and Observational study (BRAVO), *Atmos. Environ.*, *36*, 5043–5055.

Hand, J. L. et al. (2004), Single particle analyis during the Yosemite Aerosol Characterization Study, paper presented at Regional and Global Perspectives on Haze: Causes, Consequences and Controversies Visibility Specialty Conference, Air and Waste Manage. Assoc., Asheville, N. C.

Hansen, A. D. A., H. Rosen, and T. Novakov (1984), The aethalometer - An instrument for the real-time measurement of optical-absorption by aerosol-particles, *Sci. Total Environ.*, *36*, 191–196.

Hering, S. V., and P. H. McMurry (1991), Optical counter response to monodisperse atmospheric aerosols, *Atmos. Environ., Part A*, *25*, 463–468.

Iacobellis, S. F., R. Frouin, and R. C. J. Somerville (1999), Direct climate forcing by biomass-burning aerosols: Impact of correlations between controlling variables, *J. Geophys. Res.*, *104*, 12,031–12,045.

Lee, T., S. M. Kreidenweis, and J. L. Collett Jr. (2004), Aerosol ion characteristics during the Big Bend Regional Aerosol and Visibility Observational study, *J. Air Waste Manage. Assoc.*, *54*, 585–592.

Lim, H. J., B. J. Turpin, E. Edgerton, S. V. Hering, G. Allen, H. Maring, and P. Solomon (2003), Semicontinuous aerosol carbon measurements: Comparison of measurements, *J. Geophys. Res.*, *108*(D7), 8419, doi:10.1029/2001JD001214.

Malm, W. C., and D. E. Day (2000), Optical properties of aerosols at Grand Canyon National Park, *Atmos. Environ.*, *34*, 3373–3391.

Malm, W. C., and M. L. Pitchford (1997), Comparison of calculated sulfate scattering efficiencies as estimated from size-resolved particle measurements at three national locations, *Atmos. Environ.*, *31*(9), 1315–1325.

Malm, W. C., J. F. Sisler, D. Huffman, R. A. Eldred, and T. A. Cahill (1994), Spatial and seasonal trends in particle concentration and optical extinction in the U.S., *J. Geophys. Res.*, *99*, 1347–1370.

Malm, W. C., D. E. Day, and S. M. Kreidenweis (2000), Light scattering characteristics of aerosols as a function of relative humidity: part I: A

comparison of measured scattering and aerosol concentrations using the theoretical models, *J. Air Waste Manage. Assoc.*, *50*, 686–700.

Malm, W. C., D. E. Day, S. M. Kreidenweis, J. L. Collett Jr., and T. Lee (2003), Humidity dependent optical properties of fine particles during the Big Bend Regional Aerosol and Visibility study (BRAVO), *J. Geophys. Res.*, *108*(D9), 4279, doi:10.1029/2002JD002998.

Malm, W. C., B. A. Schichtel, M. L. Pitchford, L. L. Ashbaugh, and R. A. Eldred (2004), Spatial and monthly trends in speciated fine particle concentration in the United States, *J. Geophys. Res.*, *109*, D03306, doi:10.1029/2003JD003739.

Marple, V. A., K. L. Rubow, and S. M. Behm (1991), A micro-orifice uniform deposit impactor (MOUDI) - Description, calibration, and use, *Aerosol Sci. Technol.*, *14*, 434–446.

McMeeking, G. R., S. M. Kreidenweis, C. Carrico, T. Lee, J. L. Collett Jr., and W. C. Malm (2005), Smoke influenced aerosol observations during the Yosemite Aerosol Characterization Study: Size distributions and chemical composition, *J. Geophys. Res.*, *110*, D09206, doi:10.1029/2004JD005389.

Molenar, J. V. (1997), Analysis of the real world performance of the Optec NGN-2 ambient nephelometers, in *Visual Air Quality: Aerosols and Global Radiation Balance*, pp. 243–265, Air and Waste Manage. Assoc., Pittsburgh, Pa.

Molenar, J. V., D. L. Dietrich, and R. M. Tree (1989), Application of a long range transmissometer to measure the ambient atmospheric extinction coefficient in remote pristine environments, in *Transactions Visibility and Fine Particles*, edited by C. V. Mathai, Air and Waste Manage. Assoc., Pittsburgh, Pa.

Orsini, D. A., Y. L. Ma, A. Sullivan, B. Sierau, K. Baumann, and R. J. Weber (2003), Refinements to the particle-into-liquid sampler (PILS) for ground and airborne measurements of water soluble aerosol composition, *Atmos. Environ.*, *37*, 1243–1259.

Penner, J. E., R. E. Dickinson, and C. A. O'Neill (1992), Effects of aerosol from biomass burning on the global radiation budget, *Science*, *256*, 1432–1434.

Rupprecht, G., H. Patashnick, D. E. Beeson, R. N. Green, and M. B. Meyer (1995), A new automated monitor for the measurement of particulate carbon in the atmosphere, presented at Conference on Particulate Matter: Health and Regulatory Issues, Air and Waste Manage. Assoc., Pittsburgh, Pa.

Sachweh, B., H. Umhauer, F. Ebert, H. Buttner, and R. Friehmelt (1998), In situ optical particle counter with improved coincidence error correction for number concentrations up to 10(7) particles cm(−3), *J. Aerosol Sci.*, *29*, 1075–1086.

Seinfeld, J. H., and S. N. Pandis (1998), *Atmospheric Chemistry and Physics: From Air Pollution to Climate Change*, pp. 969–971, John Wiley, Hoboken, N. J.

Stolzenburg, M., N. Kreisberg, and S. Hering (1998), Atmospheric size distributions measured by differential mobility optical particle size spectrometry, *Aerosol Sci. Technol.*, *29*, 402–418.

Trijonis, J. C., W. C. Malm, M. Pitchford, W. H. White, R. Charlson, and R. Husar (1990), Visibility: Existing and historical conditions—Causes and effects, *Rep. 24*, Natl. Acid Precip. Assess. Program, Washington, D. C.

Turpin, B. J., and H. J. Lim (2001), Species contribution to PM2.5 mass concentrations: Revisiting common assumptions for estimating organic mass, *Aerosol Sci. Technol.*, *35*(1), 602–610.

Twitty, J. T., and J. A. Weinman (1971), Radiative properties of carbonaceous aerosols, *J. Appl. Meteorol.*, *10*, 725–731.

U.S. Environmental Protection Agency (1999), Regional haze regulations: Final rule, 40 CFR Part 51, 64(126), *Docket A-95-38*, Federal Register, Washington, D. C.

U.S. Environmental Protection Agency (2003), Guidance for tracking progress under the regional haze rule, *EPA-454/B-03-004*, Off. of Air Qual. Plann. and Stand., Research Triangle Park, N. C.

Weber, R., et al. (2003), Intercomparison of near real time monitors of PM2.5 nitrate and sulfate at the U.S. Environmental Protection Agency Atlanta Supersite, *J. Geophys. Res.*, *108*(D7), 8421, doi:10.1029/2001JD001220.

White, W. H., and P. T. Roberts (1977), On the nature and origins of visibility-reducing aerosols in the Los Angeles air basin, *Atmos. Environ.*, *11*, 803–812.

Zhang, X. Q., P. H. McMurry, S. V. Hering, and G. S. Casuccio (1993), Mixing characteristics and water content of submicron aerosols measured in Los Angeles and at the Grand Canyon, *Atmos. Environ., Part A*, *27*, 1593–1607.

C. Carrico, J. Carrillo, J. L. Collett Jr., S. M. Kreidenweis, T. Lee, and G. McMeeking, Department of Atmospheric Science, Colorado State University, Fort Collins, CO 80523, USA.

D. E. Day, Cooperative Institute for Research in the Atmosphere, Colorado State University, Fort Collins, CO 80523, USA.

W. C. Malm and B. Schichtel, National Park Service-Air Resources Division, Cooperative Institute for Research in the Atmosphere, Colorado State University, Fort Collins, CO 80523, USA. (malm@cira.colostate.edu)